Cell Reports
Medicine

Article

IL-7-primed bystander CD8 tumor-infiltrating lymphocytes optimize the antitumor efficacy of T cell engager immunotherapy

Graphical abstract

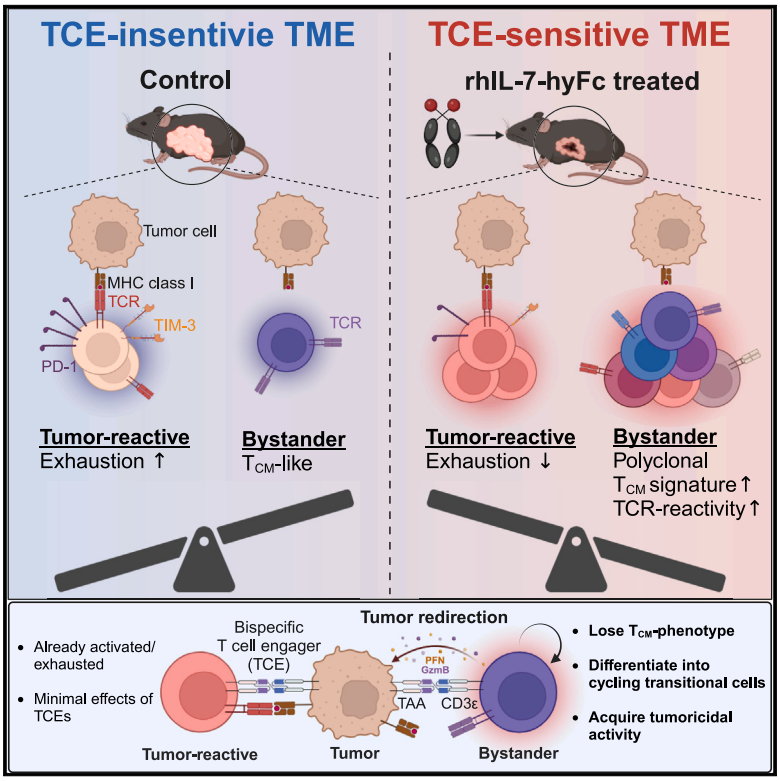

Highlights

- IL-7-Fc treatment increases PD-1-negative bystander CD8 TILs within solid tumors
- IL-7-Fc-induced bystander CD8 TILs display a non-exhausted central memory phenotype
- TCE redirects IL-7-Fc-induced bystander CD8 TILs to acquire tumoricidal activity
- IL-7-Fc optimizes the antitumor effects of TCEs by reshaping CD8 TIL populations

Authors

Kun-Joo Lee, Donghoon Choi, Nara Tae, ..., Sun Shim Choi, Dae Hee Kim, Seung-Woo Lee

Correspondence

schoi@kangwon.ac.kr (S.S.C.), kimdh@kangwon.ac.kr (D.H.K.), sw_lee@postech.ac.kr (S.-W.L.)

In brief

Though promising in cancer immunotherapy, bispecific T cell engagers (TCEs) face challenges in treating solid tumors. Lee et al. demonstrate that IL-7-Fc treatment enhances the antitumor efficacy of TCE immunotherapy in solid tumors by increasing TCE-sensitive CD8 tumor-infiltrating lymphocytes, suggesting a strategy for optimizing TCE immunotherapy with IL-7-Fc.

Lee et al., 2024, Cell Reports Medicine 5, 101567
May 21, 2024
https://doi.org/10.1016/j.xcrm.2024.101567

CellPress

Cell Reports Medicine

CellPress
OPEN ACCESS

Article

IL-7-primed bystander CD8 tumor-infiltrating lymphocytes optimize the antitumor efficacy of T cell engager immunotherapy

Kun-Joo Lee,[1,9] Donghoon Choi,[2,9] Nara Tae,[3] Ha Won Song,[4] Yeon-Woo Kang,[1] Minji Lee,[2] Dain Moon,[1] Youngsik Oh,[1] Sujeong Park,[1] Ji-Hae Kim,[1] Siheon Jeong,[1] Jaehyuk Yang,[1] Uni Park,[1] Da Hee Hong,[5] Mi-Sun Byun,[5] Su-Hyung Park,[6] Joohyuk Sohn,[7] Yunji Park,[1] Sun-Kyoung Im,[2] Sun Shim Choi,[4,*] Dae Hee Kim,[3,8,*] and Seung-Woo Lee[1,10,*]

[1]Department of Life Sciences, Pohang University of Science and Technology, Pohang 37673, Republic of Korea
[2]Research Institute of NeoImmuneTech, Inc., Pohang 37673, Republic of Korea
[3]Kangwon Institute of Inclusive Technology, Kangwon National University, Chuncheon 24341, Republic of Korea
[4]Division of Biomedical Convergence, College of Biomedical Science, Institute of Bioscience & Biotechnology, Kangwon National University, Chuncheon 24341, Republic of Korea
[5]Genexine Inc., Seoul 07789, Republic of Korea
[6]Graduate School of Medical Science and Engineering, Korea Advanced Institute of Science and Technology, Daejeon 34141, Republic of Korea
[7]Division of Medical Oncology, Department of Internal Medicine, Yonsei Cancer Center, Yonsei University College of Medicine, Seoul 03722, Republic of Korea
[8]College of Pharmacy, Kangwon National University, Chuncheon 24341, Republic of Korea
[9]These authors contributed equally
[10]Lead contact
*Correspondence: schoi@kangwon.ac.kr (S.S.C.), kimdh@kangwon.ac.kr (D.H.K.), sw_lee@postech.ac.kr (S.-W.L.)
https://doi.org/10.1016/j.xcrm.2024.101567

SUMMARY

Bispecific T cell engagers (TCEs) show promising clinical efficacy in blood tumors, but their application to solid tumors remains challenging. Here, we show that Fc-fused IL-7 (rhIL-7-hyFc) changes the intratumoral CD8 T cell landscape, enhancing the efficacy of TCE immunotherapy. rhIL-7-hyFc induces a dramatic increase in CD8 tumor-infiltrating lymphocytes (TILs) in various solid tumors, but the majority of these cells are PD-1-negative tumor non-responsive bystander T cells. However, they are non-exhausted and central memory-phenotype CD8 T cells with high T cell receptor (TCR)-recall capacity that can be triggered by tumor antigen-specific TCEs to acquire tumoricidal activity. Single-cell transcriptome analysis reveals that rhIL-7-hyFc-induced bystander CD8 TILs transform into cycling transitional T cells by TCE redirection with decreased memory markers and increased cytotoxic molecules. Notably, TCE treatment has no major effect on tumor-reactive CD8 TILs. Our results suggest that rhIL-7-hyFc treatment promotes the antitumor efficacy of TCE immunotherapy by increasing TCE-sensitive bystander CD8 TILs in solid tumors.

INTRODUCTION

CD8 T cells play a pivotal role in the antitumor immune response by directly targeting and eliminating tumor cells expressing tumor antigens.[1,2] However, tumor suppression by tumor-reactive CD8 T cells can be hindered by T cell exhaustion or dysfunction, in which continuous antigen stimulation along with the signals from immune checkpoint molecules, such as cytotoxic T lymphocyte-associated antigen 4 (CTLA-4) and programmed cell death 1 (PD-1), gradually impairs T cell activity. Despite the clinical success of immune checkpoint inhibitors (ICIs),[3] the response rate in many cancer patients remains still low.[4] Also, therapeutic strategies to increase the activity of tumor-reactive T cells are ineffective in situations where tumor antigen expression is limited,[5,6] emphasizing the demand for innovative immunotherapies with improved efficacy.

Bispecific T cell engagers (TCEs) are designed to simultaneously bind tumor cells and T cells, bridging them together and enhancing T cell activation and tumor cell killing. TCEs can redirect T cells to tumor cells in a T cell receptor (TCR)-independent manner, enabling activation of T cells with diverse TCR specificities[7] even in tumors with low expression of major histocompatibility complex class I molecule.[8] The dynamic interaction between tumor and immune cells in the hematological system facilitates the potent antitumor actions of TCEs, leading to their remarkable success.[9] In 2014, the Food and Drug Administration approved Blinatumomab, an anti-CD19×anti-CD3 TCE, for treating precursor B cell acute lymphoblastic leukemia.[10] More recently, an anti-BCMA×anti-CD3 (Teclistamab) and anti-gp100×anti-CD3 (Tebentafusp) TCEs were also approved for patients with relapsed or refractory multiple myeloma (MM) and metastatic uveal melanoma, respectively.[11,12] However,

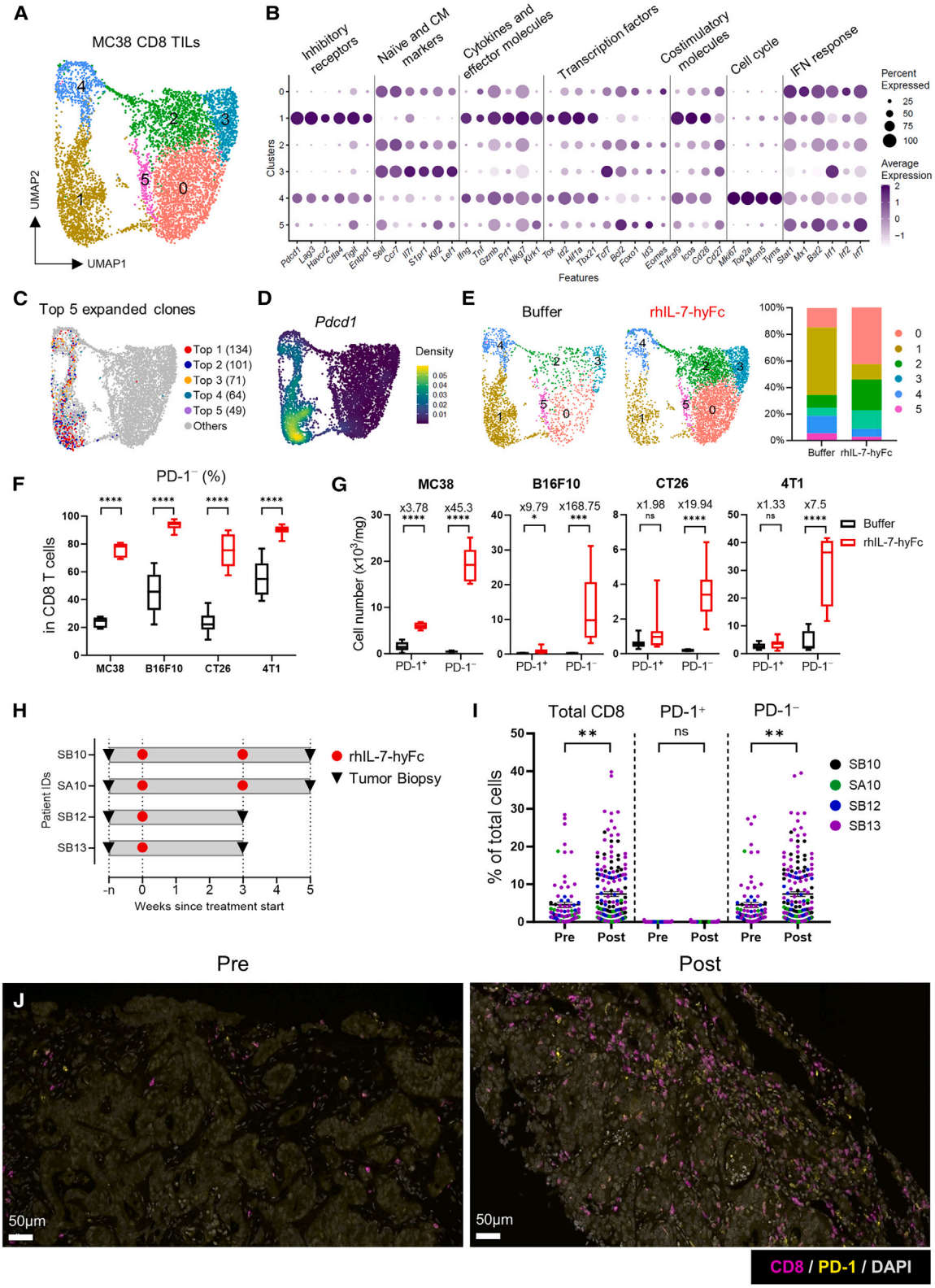

Figure 1. rhIL-7-hyFc treatment increases PD-1⁻ bystander CD8 TILs

(A–E) scRNA-seq analysis of CD8 TILs. Mice bearing palpable MC38 tumors treated subcutaneously (s.c.) with rhIL-7-hyFc (10 mg kg^{-1}). Tumors were collected 7 days after rhIL-7-hyFc treatment. Collected tumor tissues were pooled for analysis (n = 5–7 per group). Unless specified otherwise, the data include TILs from

(legend continued on next page)

even in hematologic malignancies, TCEs face several challenges, including cytokine release syndrome, loss of tumor antigens, on-target off-tumor toxicity, and suboptimal potency.[13–15] It is widely acknowledged that their antitumor efficacy is even lower in solid tumors compared with hematologic cancers. The application of TCEs in solid tumors is hindered by immunosuppressive tumor microenvironments (TMEs) characterized by T cell exhaustion, immunosuppressive cells, and limited T cell infiltration.[16–19] Therefore, combination with other therapies that can overcome the immunosuppressive TME environment in solid cancers may increase the efficacy of TCE-mediated immunotherapy.

Not only antigen-specific but also bystander CD8 T cells that do not recognize tumor antigens are found within the TMEs.[20,21] Bystander T cells can infiltrate tumor tissues because the chemotactic process promotes T cell recruitment to inflammatory sites.[22,23] Importantly, bystander cells are not exhausted as they remain ignorant of tumor cells,[24] as evidenced by low expression levels of checkpoint receptors such as PD-1, lymphocyte activating gene 3 (LAG-3) and CD39 (encoded by *ENTPD1*) in both preclinical and clinical contexts.[24–26] Therefore, bystander CD8 T cells in tumors can show functionality in response to cognate antigen stimulation,[27,28] and some studies suggest that activating bystander CD8 T cells within the TME improves antitumor responses,[29–31] indicating their therapeutic potential.

Interleukin-7 (IL-7) plays a crucial role in T cell development, differentiation, and survival. Therefore, recombinant IL-7 has been explored as an immunotherapeutic agent,[32–34] but its short half-life and low productivity have limited its pharmaceutical efficacy. rhIL-7-hyFc (NT-I7; efineptakin alfa), a long-acting form of recombinant human IL-7 fused with the hybrid-Fc fragment, offers increased stability and an extended half-life.[35] In several mouse tumor models, we and others have demonstrated that rhIL-7-hyFc treatment showed antitumor activity by promoting an inflamed TME and increased the antitumor efficacy when combined with chemotherapy, radiotherapy, and ICIs.[36,37] With promising results in the preclinical models, rhIL-7-hyFc is currently being evaluated in clinical trials for multiple cancer types as a monotherapy and in combination with ICIs (NCT05465954, NCT04984811, NCT04893018). It is evident that the antitumor effects of rhIL-7-hyFc are related to the increased number and activity of CD8 T cells; however, the detailed mechanism by which rhIL-7-hyFc regulates the differentiation and function of CD8 tumor-infiltrating lymphocytes (TILs) has not been clearly understood. In this study, we showed through single-cell RNA sequencing (scRNA-seq) analysis that rhIL-7-hyFc treatment significantly increased bystander CD8 T cells with high TCR-recall potential in tumors. We propose TCE immunotherapy as a way to harness rhIL-7-hyFc-induced bystander CD8 TILs for antitumor responses. TCEs were able to redirect IL-7-increased bystander CD8 TILs to tumor cells and differentiated them into a subset with cytotoxic activity. Therefore, the combination of rhIL-7-hyFc and TCE treatments exhibited improved antitumor efficacy in various solid tumor models by increasing the number of CD8 TILs capable of exerting tumoricidal function.

RESULTS

rhIL-7-hyFc monotherapy increases PD-1$^-$ CD8 TILs in mice and humans

In our previous research, we demonstrated that rhIL-7-hyFc monotherapy exhibits significant antitumor activity against MC38 colorectal tumors, a widely used immunogenic model for evaluating immunotherapeutic agents. The antitumor effect of rhIL-7-hyFc is entirely dependent on CD8 T cells, with CD4 T cells and natural killer (NK) cells having no significant impact.[36] Building on these findings, our follow-up study aims to delve deeper into the mechanisms by which rhIL-7-hyFc modulates the composition and functionality of CD8 T cells within the tumor, thereby enhancing our understanding of its therapeutic potential in tumor immunotherapy. To examine changes in the composition and function of CD8 TILs after rhIL-7-hyFc treatment, we performed ascRNA-seq paired with single-cell TCR sequencing (scTCR-seq) analysis by collecting CD8 TILs from MC38 tumor-bearing mice after rhIL-7-hyFc or buffer treatment. Six clusters of CD8 TILs were identified by Seurat-based clustering (Figures 1A and S1A). Cells in clusters 1 and 4 highly expressed inhibitory receptors (*Pdcd1*, *Havcr2*, *Entpd1*), effector molecules (*Gzmb*, *Prf1*, *Ifng*), and costimulatory molecules (*Tnfrsf9, Icos, Cd28*) but low levels of naive and central memory (CM) markers (*Ccr7*, *Sell*). In addition, both clusters increased the expression of T cell exhaustion-related transcription factors (TFs) such as *Id2*, *Tbx21,* and *Tox* (Figures 1B and S1B). These transcriptomic profiles suggest that CD8 TILs in clusters 1 and 4 are tumor-reactive. The distribution of the top five clonally expanded cells supported that clusters 1 and 4 consist of tumor-reactive cells (Figure 1C). Cells in cluster 4 resembled progenitor-exhausted cells with strong expression of cell cycle genes, although *Tcf7*

both buffer- and rhIL-7-hyFc-treated mice. (A) UMAP plots of six distinct CD8 TIL clusters from MC38-bearing mice, numbered and colored according to the transcriptional clusters. (B) Dot plot showing the expression of various T cell-related genes in the six different clusters. (C) UMAP plot of top five expanded clones. (D) UMAP showing the distribution of expression of *Pdcd1* transcript. (E) UMAP showing CD8 TIL clusters from buffer- or rhIL-7-hyFc-treated mice (left) and bar graph depicting the proportion of six clusters in each treatment condition (right).

(F and G) rhIL-7-hyFc (10 mg kg^{-1}) were treated s.c. in mice bearing various palpable tumors. Tumors were collected 7 days after rhIL-7-hyFc treatment (n = 5–11 per group). (F) Frequency of PD-1$^-$ CD8 T cells among total CD8 TILs. (G) Number of PD-1$^+$ CD8 T cells (left) and PD-1$^-$ CD8 T cells (right). Numbers on the bar indicate fold changes between buffer- and rhIL-7-hyFc-treated groups. Data are shown as mean ± SEM and representative of two independent experiments.

(H) Schematic of clinical study design. Patients with metastatic colorectal and ovarian cancer were treated with rhIL-7-hyFc. Pre- and post-treatment tumor samples were collected during the screening period and at indicated time points.

(I) Percentage of total CD8 T cells (left), PD-1$^+$ CD8 T cells (middle), and PD-1$^-$ CD8 T cells (right) among the total cells. Each dot represents a single region of interest (ROI) in each patient's sample. The ROIs were manually designated by pathologists.

(J) Representative immunofluorescence images of tumor biopsies from patient SB13. Purple, CD8; yellow, PD-1; gray, DAPI. Magnification, ×200, scale bars, 50 μm *p < 0.05, **p < 0.01, ***p < 0.001, and ****p < 0.0001 by unpaired (F, G, and I) two-tailed Student's t test. See also Figures S1; Table S1.

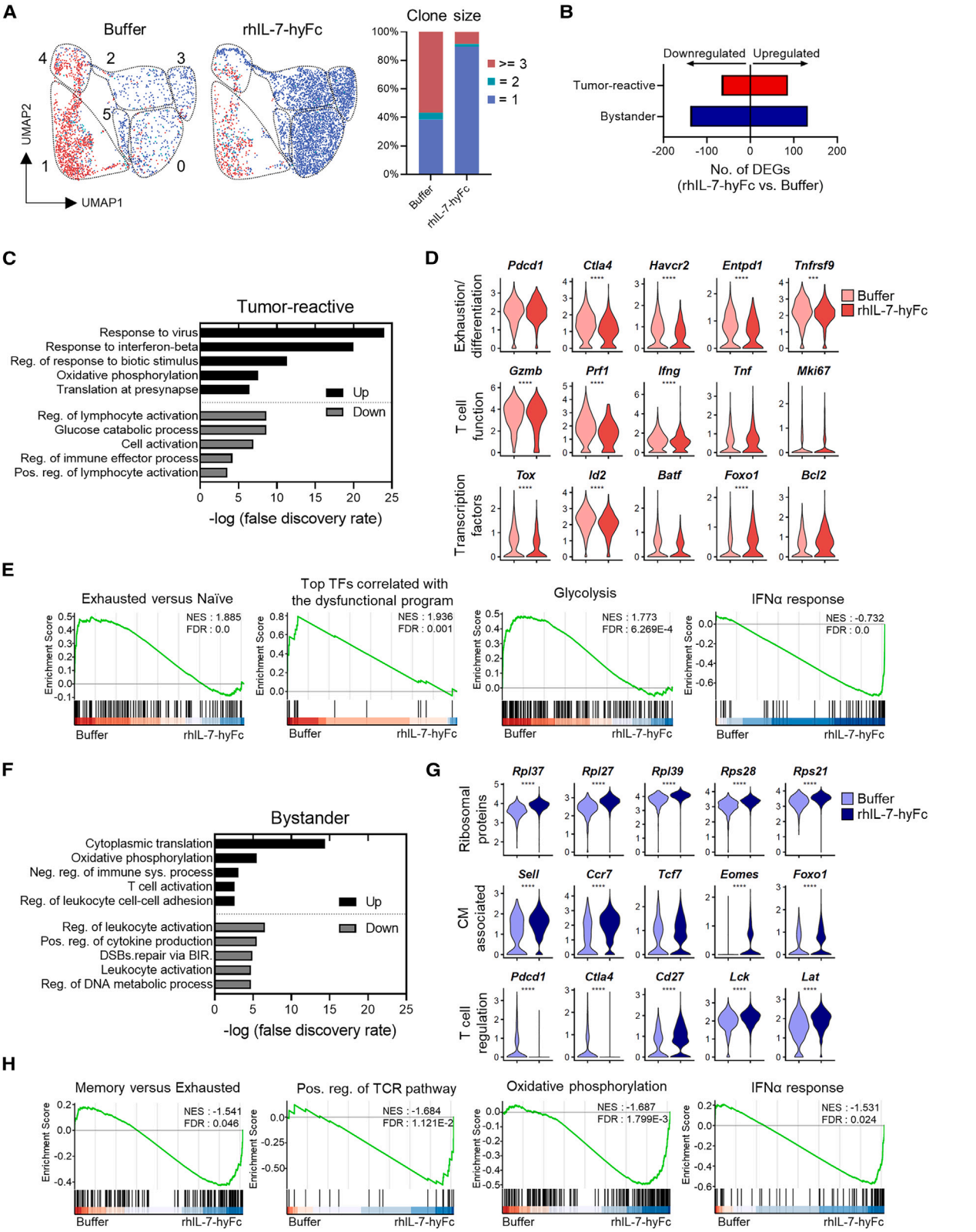

(legend on next page)

expression was minimal. Cluster 1 cells exhibited terminally differentiated/exhausted characteristics, with significantly high expression of exhaustion-related genes and effector molecules (Figures 1B and S1B). Cells in clusters 0, 2, 3, and 5, on the other hand, showed substantial expression of naive and CM markers but not exhaustion-related or effector molecules, indicating that such CD8 TILs are not tumor-reactive but bystander cells (Figures 1B and S1B). *Pdcd1* transcript expression, a marker for T cell exhaustion and tumor reactivity,[38] distinguished tumor-reactive CD8 TILs as expected (Figure 1D). rhIL-7-hyFc treatment dramatically altered the composition of CD8 TILs by increasing PD-1$^-$ bystander cells such as clusters 0, 2, and 3, while reducing the proportion of PD-1$^+$ tumor-reactive cells in clusters 1 and 4 (Figure 1E).

To assess whether rhIL-7-hyFc treatment leads to an increase in PD-1$^-$ bystander CD8 TILs across various tumor models with differing genetic backgrounds and immunogenic potentials, mice bearing palpable B16F10, CT26, and 4T1 tumors were treated with rhIL-7-hyFc. Flow cytometry analysis was subsequently conducted to evaluate the composition of CD8 TILs, utilizing the MC38 tumor model as a control. The analysis revealed that rhIL-7-hyFc therapy specifically led to dramatic increases in the proportion of PD-1$^-$ CD8 TILs in all tested tumor models (Figure 1F). When examined in absolute numbers, rhIL-7-hyFc induced a slight increase in PD-1$^+$ CD8 TILs only in highly immunogenic MC38 tumors but no significant expansion in less or poorly immunogenic tumors, including CT26, B16F10, and 4T1. In sharp contrast, rhIL-7-hyFc treatment dramatically enhanced PD-1$^-$ CD8 TILs independent of tumor types (Figure 1G). As we previously demonstrated that rhIL-7-hyFc administration preferentially amplified CM-phenotype CD8 T cells in the periphery and trafficked them into tumors via chemokine receptors,[36] our findings suggest that rhIL-7-hyFc-induced PD-1$^-$ CD8 TILs in various tumors are recruited from the periphery and reside as bystander T cells.

It has been reported that rhIL-7-hyFc administration in both healthy adults and cancer patients leads to a dose-dependent increase in absolute lymphocyte count (ALC), CD4, and CD8 T cell counts in the peripheral blood (PB).[39,40] To determine whether this increase in blood CD8 T cells reflects changes within the tumor microenvironment, we analyzed tumor tissues from four patients with metastatic colorectal and ovarian cancer after rhIL-7-hyFc treatment using immunohistochemistry (IHC). This analysis enabled us to assess the quantity and phenotype of CD8 T cells (Figure 1H; Table S1). The rhIL-7-hyFc treatment was associated with an increased frequency of CD8 T cells within the tumors. More significantly, the majority of CD8 T cells raised by rhIL-7-hyFc were PD-1-negative (Figures 1I and 1J). These results indicate that rhIL-7-hyFc therapy promotes PD-1$^-$ CD8 TILs in human tumors.

rhIL-7-hyFc attenuates T cell exhaustion in tumor-reactive CD8 TILs and augments TCR-responsiveness in bystander CD8 TILs

Next, we analyzed the transcriptomic changes of CD8 TILs to examine how rhIL-7-hyFc treatment affects T cell differentiation and function within tumors. Although we classified CD8 TILs as PD-1$^+$ tumor-reactive vs. PD-1$^-$ bystander cells, we used scTCR-seq data from individual CD8 TIL to distinguish the two populations based on clone size, a reflection of antigen-driven expansion and a recognized marker of tumor reactivity.[41,42] Thus, we grouped tumor-reactive cells with a clone size of 3 or more, which were mainly found in UMAP (Uniform Manifold Approximation and Projection) clusters 1 and 4. In contrast, bystander cells with a clone size of 1 and 2 were located in clusters 0, 2, and 3 (Figure 2A). The two groups had very distinctive gene-expression profiles; tumor-reactive cells overexpressed genes associated with T cell exhaustion, whereas bystander cells overexpressed CM-associated genes (Figure S2A). We found that around 60% of CD8 TILs in buffer-treated mice were identified as tumor-reactive cells, but more than 80% of CD8 TILs were bystander cells in rhIL-7-hyFc-treated mice (Figure 2A).

rhIL-7-hyFc treatment induced transcriptomic changes in both groups of CD8 TILs, albeit bystander cells had a higher number of differentially expressed genes (DEGs) than tumor-reactive cells (Figure 2B; Table S2). According to Gene Ontology (GO) analysis, rhIL-7-hyFc treatment upregulated genes involved in antiviral/IFN-β response and oxidative phosphorylation while downregulating genes involved in lymphocyte activation and glycolysis in tumor-reactive cells (Figure 2C). As lymphocyte activation of CD8 T cells within tumors includes a continuous process from cellular activation to terminal differentiation or exhaustion, tumor-reactive CD8 TILs isolated from rhIL-7-hyFc-treated mice expressed lower levels of immune checkpoint molecules (*Ctla4*, *Havcr2, Entpd1, Tnfrsf9*), effector molecules (*Gzmb*, *Prf1, Ifng*), and TFs associated with T cell exhaustion (*Tox*, *Id2*) (Figure 2D). Protein levels of key immune checkpoint

Figure 2. rhIL-7-hyFc treatment changes the transcriptome profiles of tumor-reactive and bystander CD8 TILs

(A) UMAP of scTCR-seq data colored according to the clone size of expanded CD8 TILs from mice bearing MC38 tumors between groups (left) and a bar graph showing the proportion of CD8 TILs with each clone size between groups (right).

(B) Number of DEGs in tumor-reactive and bystander CD8 TILs from tumor-bearing mice with rhIL-7-hyFc treatment compared with buffer treatment.

(C) Top 5 enriched GO terms for up- or downregulated genes in tumor-reactive cells by rhIL-7-hyFc treatment.

(D) Violin plots with an expression of genes related to T cell exhaustion, function, and TFs in tumor-reactive cells.

(E) GSEA analysis with the gene set of exhausted vs. naive CD8 T cells (GEO: GSE9650), top TFs correlated with the dysfunctional program (Li et al.[24]), glycolysis (MSigDB: hallmark), and IFN-alpha response (MSigDB: hallmark) in tumor-reactive CD8 TILs.

(F) Top 5 enriched GO terms for up- or downregulated genes in bystander cells by rhIL-7-hyFc treatment.

(G) Violin plots with expression of genes related to ribosomal proteins, CM T cell, and T cell regulation in bystander cells.

(H) GSEA analysis with the gene set of memory vs. exhausted CD8 T cells (GEO: GSE9650), positive regulation of TCR pathway (GO: 0050862), oxidative phosphorylation (MSigDB: hallmark), and IFN-alpha response (MSigDB: hallmark) in bystander CD8 TILs. Tumor-reactive cells are defined as cells with a clone size of 3 or greater, and bystander cells are defined as cells with a clone size of 1 or 2 and belonging to one of clusters 0, 2, 3, and 5. BIR., break-induced replication; DSBs., double-strand breaks; neg., negative; reg., regulation; sys., system; Pos., positive. See also Figures S2 and S3; Table S2.

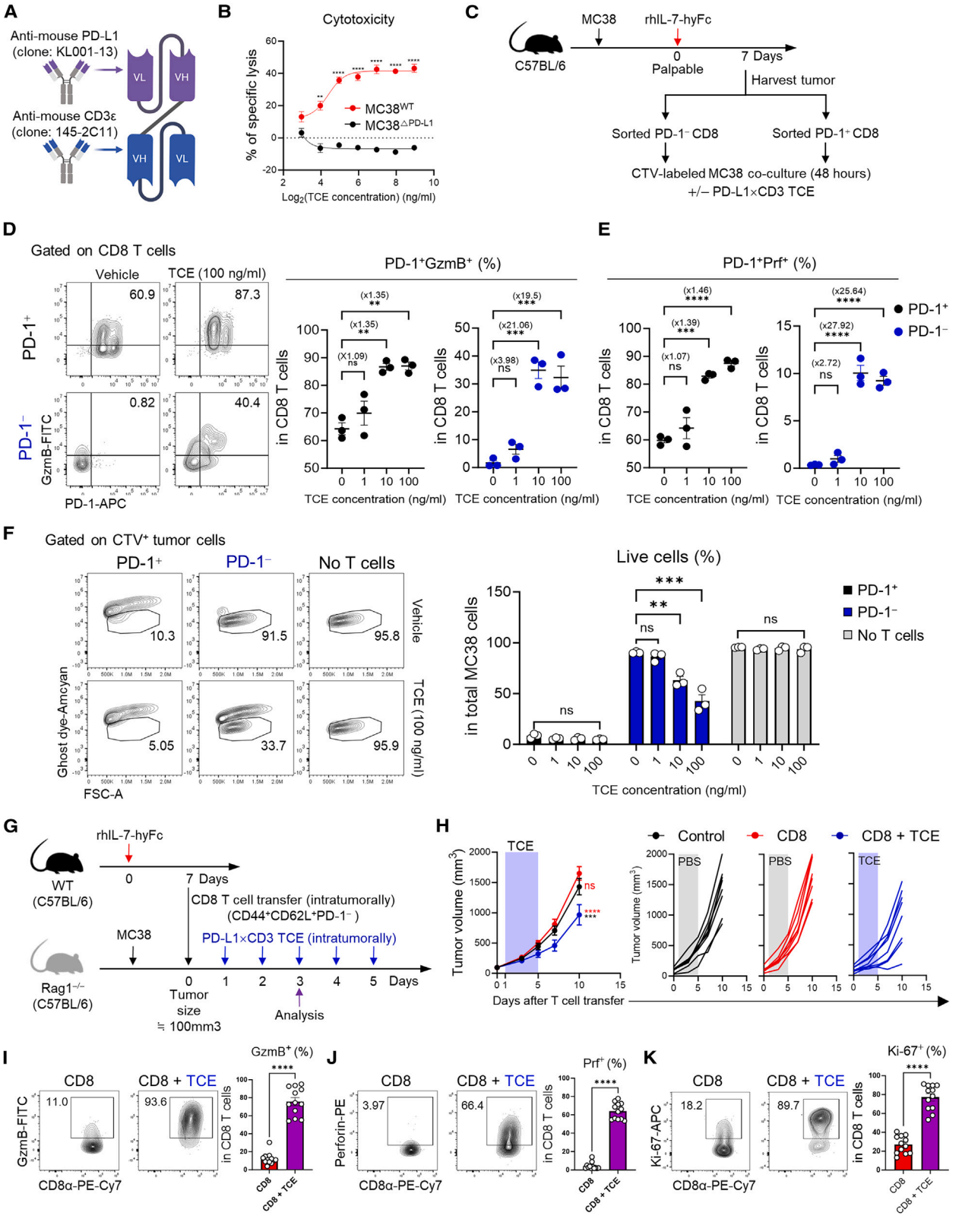

(legend on next page)

receptors and effector molecules in PD-1$^+$ tumor-reactive CD8 TILs were further validated by flow cytometry (Figures S2B and S2C). Gene set enrichment analysis (GSEA) further confirmed that rhIL-7-hyFc-stimulated tumor-reactive CD8 TILs had reduced enrichment scores in gene sets associated with T cell exhaustion/dysfunction, and glycolysis (Figure 2E). Since glycolysis is a more preferred metabolic pathway during T cell exhaustion than oxidative phosphorylation,[43–45] our transcriptome study implies that rhIL-7-hyFc treatment attenuates terminal differentiation and exhaustion of tumor-antigen responding CD8 TILs.

In the bystander T cells, the most noticeable change was a rise in cytoplasmic translation-related genes, including ribosomal proteins (Figures 2F and 2G). Memory T cells have a higher concentration of ribosomal protein than naive T cells, which allows them to respond to recall antigens more quickly due to faster protein translation.[46] Furthermore, rhIL-7-hyFc treatment increased the expression of CM-associated genes (*Sell*, *Ccr7*, *Eomes, Foxo1*) and T cell activation genes (*Cd27, Lck, Lat*) in bystander cells (Figure 2G). On the contrary, rhIL-7-hyFc treatment lowered the expression of genes linked with leukocyte activation regulation, such as *Pdcd1* and *Ctla4*, even though the expression level of those genes was much lower in bystander cells than in tumor-reactive cells (Figures 2F and 2G). Again, protein levels of CM-associated molecules and immune checkpoint molecules in PD-1$^-$ bystander CD8 TILs were further confirmed by flow cytometry (Figures S2D and S2E). GSEA further supported that bystander CD8 TILs induced by rhIL-7-hyFc had higher enrichment scores in gene sets related to T cell memory, TCR pathway, and oxidative phosphorylation (Figure 2H). Therefore, rhIL-7-hyFc-stimulated bystander CD8 TILs are CM-phenotype cells with non-exhausted but a high capacity for recall response. Noticeably, rhIL-7-hyFc treatment increased genes related to type-I IFN response in both tumor-reactive and bystander CD8 TILs (Figures 2E and 2H; Table S2). A previous report has demonstrated that IL-7-dependent STAT1 activation and the elevation of IFN-stimulated genes (ISGs) in the lymphopenia-induced proliferation of CD4 T cells,[47] suggesting that rhIL-7-hyFc treatment enhances STAT1 signaling and ISG expression in CD8 TILs.

Bispecific TCE enables rhIL-7-hyFc-induced bystander CD8 TILs to acquire cytotoxicity and antitumor activity

We next determined whether the antitumor efficacy of rhIL-7-hyFc depended on the continuous infiltration of CD8 T cells into the tumor via the PB. FTY720, a sphingosine-1-phosphate (S1P) analogue, prevents lymphocyte egress from secondary lymphoid tissues by inducing the internalization and subsequent degradation of S1P receptors.[48] Thus, we administered FTY720 to tumor-bearing mice along with rhIL-7-hyFc treatment to inhibit CD8 T cell trafficking from the PB to tumor sites, aiming to assess the impact of this blockade on the antitumor activity mediated by rhIL-7-hyFc (Figure S3A). As expected, FTY720 treatment resulted in a significant decrease in CD8 T cells in the PB, which also reduced the number of CD8 T cells in tumors (Figure S3B). Surprisingly, FTY720 treatment did not affect the antitumor efficacy of rhIL-7-hyFc (Figure S3C). These results suggest that the antitumor effects of rhIL-7-hyFc monotherapy are primarily mediated through the regulation of tumor-resident CD8 T cells. Additionally, despite the significant infiltration of bystander CD8 T cells from the PB into tumors following rhIL-7-hyFc treatment, our findings indicate that the presence of these bystander cells may not substantially contribute to the antitumor efficacy of the treatment.

Consequently, we hypothesized that the conversion of rhIL-7-hyFc-induced bystander CD8 T cells into tumor-reactive cells could be achieved through the stimulation of these cells by a bispecific TCE, independent of tumor antigen recognition. To achieve this, we utilized a TCE composed of two single-chain variable fragments (scFvs): one targeting Programmed Death-Ligand 1 (PD-L1) as a tumor-associated antigen and the other targeting CD3ε on T cells (Figure 3A). To test the functionality of anti-human/mouse cross-reactive PD-L1×anti-mouse CD3ε TCE (PD-L1×CD3 TCE) *in vitro*, CellTrace Violet (CTV)-labeled MC38 tumor cells and splenocytes were co-cultured in the presence of PD-L1×CD3 TCE. To ensure the source of PD-L1 was exclusively from tumor cells, we used PD-L1-deficient splenocytes in the experiments. Exposure to PD-L1×CD3 TCE induced proliferation and increased the cytotoxic activity of splenic CD8 T cells *in vitro*. Notably, the effects of CD8 T cell activation were only observed when cells were co-cultured with MC38 tumor

Figure 3. TCE stimulation elicits tumoricidal activity of rhIL-7-hyFc-induced bystander CD8 TILs

(A) Schematic protein structure of PD-L1×CD3 TCE. This figure was created with BioRender.com.

(B) The cytotoxicity of PD-L1$^{-/-}$ splenocytes from naive PD-L1-deficient mice was evaluated. These splenocytes were co-cultured with CTV-labeled MC38^{WT} or MC38$^{\Delta PD-L1}$ tumor cells in the presence of TCE at indicated concentrations for 48 h (n = 3 per group).

(C–F) Functional assay of PD-L1×CD3 TCE on rhIL-7-hyFc-induced tumor-reactive and bystander CD8 TILs (n = 3 per group). (C) Experimental scheme. (D) Expression of PD-1 and GzmB in PD-1$^+$ or PD-1$^-$ CD8 T cells co-cultured with MC38 in the presence of TCE at indicated concentration (left) and frequencies of PD-1$^+$GzmB$^+$ cells among CD8 T cells. Black and blue dots indicate PD-1$^+$ and PD-1$^-$ CD8 TILs before co-culture, respectively (right). (E) Frequencies of PD-1$^+$Prf$^+$ cells among CD8 T cells. (F) Cytotoxicity of PD-1$^+$ and PD-1$^-$ CD8 T cells in the presence of TCE. The expression of ghost dye in tumor cells was measured by flow cytometry. CTV$^+$Ghost dye$^+$ cells are considered dead tumor cells.

(G–K) The functional changes and antitumor effects of rhIL-7-hyFc-expanded PD-1$^-$ bystander CD8 T cells were investigated (n = 5–7 per group). (G) Experimental scheme. MC38-bearing RAG1$^{-/-}$ mice were injected i.t. with 4 × 10^6 CD8$^+$CD44$^+$CD62L$^+$PD-1$^-$ T cells sourced from the spleen and lymph nodes of C57BL/6 mice treated with rhIL-7-hyFc (10 mg kg^{-1}). PD-L1×CD3 TCE (2 μg) or PBS was administered i.t. 5 times daily from the next day after T cell transfer. For flow cytometry analysis, tumors were collected 24 h after the second TCE treatment. (H) Average (left) and individual (right) tumor growth curves of MC38-bearing RAG1$^{-/-}$ mice. The timing of TCE or PBS administration is indicated by blue or gray columns, respectively. (I) Representative plots showing the expression of GzmB in CD8 T cells (left) and frequency of GzmB$^+$ cells among CD8 T cells (right). (J) Representative plots showing the expression of Prf in CD8 T cells (left) and frequency of Prf$^+$ cells among CD8 T cells (right). (K) Representative plots showing the expression of Ki-67 in CD8 T cells (left) and frequency of Ki-67$^+$ cells among CD8 T cells (right). Data are shown as mean ± SEM and representative of two or three independent experiments (B, D-F, and H) or a summary of two independent experiments (I–K). *p < 0.05, **p < 0.01, ***p < 0.001, and ****p < 0.0001 by unpaired two-tailed Student's t test (B, I, J, and K), by one-way ANOVA and Tukey's multiple comparisons test (D–F), and by two-way ANOVA and Tukey's multiple comparisons test (H). ns, not significant. See also Figures S3 and S4.

cells expressing PD-L1 ($MC38^{WT}$) and were absent in co-cultures with MC38 cells lacking PD-L1 ($MC38^{\Delta PD-L1}$) (Figures 3B, S4A, and S4B). This demonstrates that cross-linking mediated by the tumor antigen (PD-L1) of the anti-CD3 scFv component is crucial for the activation of T cells by the TCE. To determine whether PD-L1×CD3 TCE can regulate the activity of rhIL-7-hyFc-induced bystander CD8 TILs, we isolated PD-1^+ tumor-reactive and PD-1^- bystander CD8 T cells from tumors after rhIL-7-hyFc treatment and co-cultured them *ex vivo* with tumor cells and PD-L1×CD3 TCE (Figure 3C). PD-1^+ tumor-reactive cells were already expressing high levels of granzyme B (GzmB), which was slightly increased by TCE treatment. By contrast, PD-1^- bystander cells minimally expressed GzmB right after isolation but acquired both PD-1 and GzmB expression after TCE treatment (Figure 3D). Similarly, the expression of perforin (Prf), another marker of cytotoxic function, was significantly increased in PD-1^- bystander cells by TCE treatment (Figure 3E). More importantly, the induction of cytotoxic molecules in bystander CD8 TILs led to an increase in actual cytotoxicity against tumor cells. Although PD-1^+ tumor-reactive cells showed higher per-cell basis cytotoxic capacity, PD-1^- bystander cells can gain sufficient cytotoxic capacity through TCE-mediated redirection of CD8 T cells toward tumor cells (Figure 3F).

Next, we sought to determine whether the redirected stimulation of bystander CD8 T cells by TCE alone could demonstrate antitumor efficacy *in vivo*. To this end, MC38 tumor cells were implanted into RAG1-deficient mice ($RAG1^{-/-}$), which lack T cells, followed by the adoptive transfer of rhIL-7-hyFc-expanded PD-1^- bystander CD8 T cells, along with daily intravenous (i.v.) administration of the PD-L1×CD3 TCE (Figure S4C). To ensure an adequate transfer of bystander T cells, we isolated these cells from the secondary lymphoid organs of rhIL-7-hyFc-treated normal mice. Tumor growth was only suppressed when TCE was given after the adoptive transfer of bystander T cells (Figure S4D). Administering PD-1^- bystander CD8 T cells and TCEs through i.v. injection may not efficiently target them to tumors, potentially limiting their interaction within the TME. To address this, we performed intratumoral (i.t.) adoptive transfers of CD8 T cells and TCEs into advanced MC38 tumor models in $RAG1^{-/-}$ mice (Figure 3G), which significantly enhanced the antitumor effects of TCE-redirected bystander CD8 T cells (Figure 3H). Further analysis of the TILs via flow cytometry revealed a marked increase in the accumulation of CD8 T cells within the tumor tissue following i.t. transfer (Figure S4E). In the absence of TCE treatment, the transferred PD-1^- bystander CD8 T cells remained PD-1-negative. Conversely, in tumors treated with TCE, there was a notable rise in PD-1 expression among CD8 T cells (Figure S4F), alongside increased expression of cytotoxic molecules such as GzmB and Prf (Figures 3I and 3J), and the proliferation marker Ki-67 (Figure 3K). These observations suggest that the transferred PD-1^- bystander CD8 T cells not only become activated but also acquire cytotoxic capabilities and proliferate in response to TCE treatment *in vivo*. Collectively, TCE can reroute rhIL-7-hyFc-induced bystander CD8 TILs toward tumors to achieve cytotoxic function and antitumor activity.

TCEs combined with rhIL-7-hyFc synergize to improve antitumor efficacy

As we verified that rhIL-7-hyFc-induced bystander CD8 TILs can be redirected into tumor-reactive cells by TCE, we next investigated whether their combined administration could increase antitumor efficacy in various tumor models. To do this, we subcutaneously administered rhIL-7-hyFc to mice with palpable or advanced tumors. Subsequently, starting from the third day after rhIL-7-hyFc treatment, we daily administered TCE for 5 days considering its short half-life due to the absence of the fragment crystallizable region (Fc region). This strategy aims to synchronize TCE action with the rhIL-7-hyFc-induced CD8 T cell expansion, starting on day 4 and peaking on day 7 post-treatment in mice.[36] To identify the final concentrations of rhIL-7-hyFc and PD-L1×CD3 TCE for a combination regimen, we first investigated several dose combinations of the two reagents based on tumor immunogenicity and therapeutic delivery route (Figure S5). rhIL-7-hyFc or TCE monotherapy in the MC38 palpable tumor model had a modest antitumor effect, but combination therapy significantly improved the antitumor response (Figure 4A). In the less immunogenic B16F10 palpable model, rhIL-7-hyFc or TCE alone had little antitumor activity, but combination therapy could significantly inhibit tumor growth (Figure 4B). Because the TCE form we used has a poor pharmacokinetics profile, the concentration of TCE within tumors is likely to be very low. Therefore, to maximize the activity of rhIL-7-hyFc-induced CD8 TILs, we administered TCE intratumorally, using the approach previously employed in experiments with $RAG1^{-/-}$ mice where adoptive transfer was performed (Figure 3G). This experiment was carried out in the advanced MC38 tumor model, as the i.t. administration of TCE required tumors of adequate size. As anticipated, i.t. administration of TCE alone induced antitumor efficacy, with combination therapy yielding even greater antitumor effects (Figure 4C).

Although PD-L1 is an antigen expressed in tumor cells, many normal cells also express PD-L1.[49] PD-L1 is expressed by numerous myeloid cells in tumors, which play an important role in the antitumor response of anti-PD-L1 antibodies.[50] More recently, the ability of T cell activation in tumors by PD-L1×CD3 bispecific antibody was unrelated to tumor cells expressing PD-L1, suggesting that the antitumor effects of PD-L1×CD3 TCE we used in this study could be caused by PD-L1 expressed in non-tumor cells, including myeloid cells within tumors.[51] Therefore, we wanted to confirm the antitumor effects of the combination of rhIL-7-hyFc with a more tumor antigen-specific TCE. We developed anti-human HER2×anti-mouse CD3ε TCE (HER2×CD3 TCE), which can target the genuine tumor-specific antigen human HER2 protein overexpressed in CT26 tumor cells ($CT26^{hHER2}$) (Figures S6A and S6B). Similarly, HER2×CD3 TCE could activate splenic CD8 T cells *in vitro* when co-cultured with $CT26^{hHER2}$ (Figures S6C and S6D). The combination treatment of rhIL-7-hyFc and HER2×CD3 TCE significantly suppressed tumor growth, but rhIL-7-hyFc or TCE monotherapy failed to generate an effective antitumor response (Figure 4D). These results suggest that the engagement of rhIL-7-hyFc-induced CD8 TILs by TCEs targeting tumor antigens is an effective strategy to augment antitumor responses.

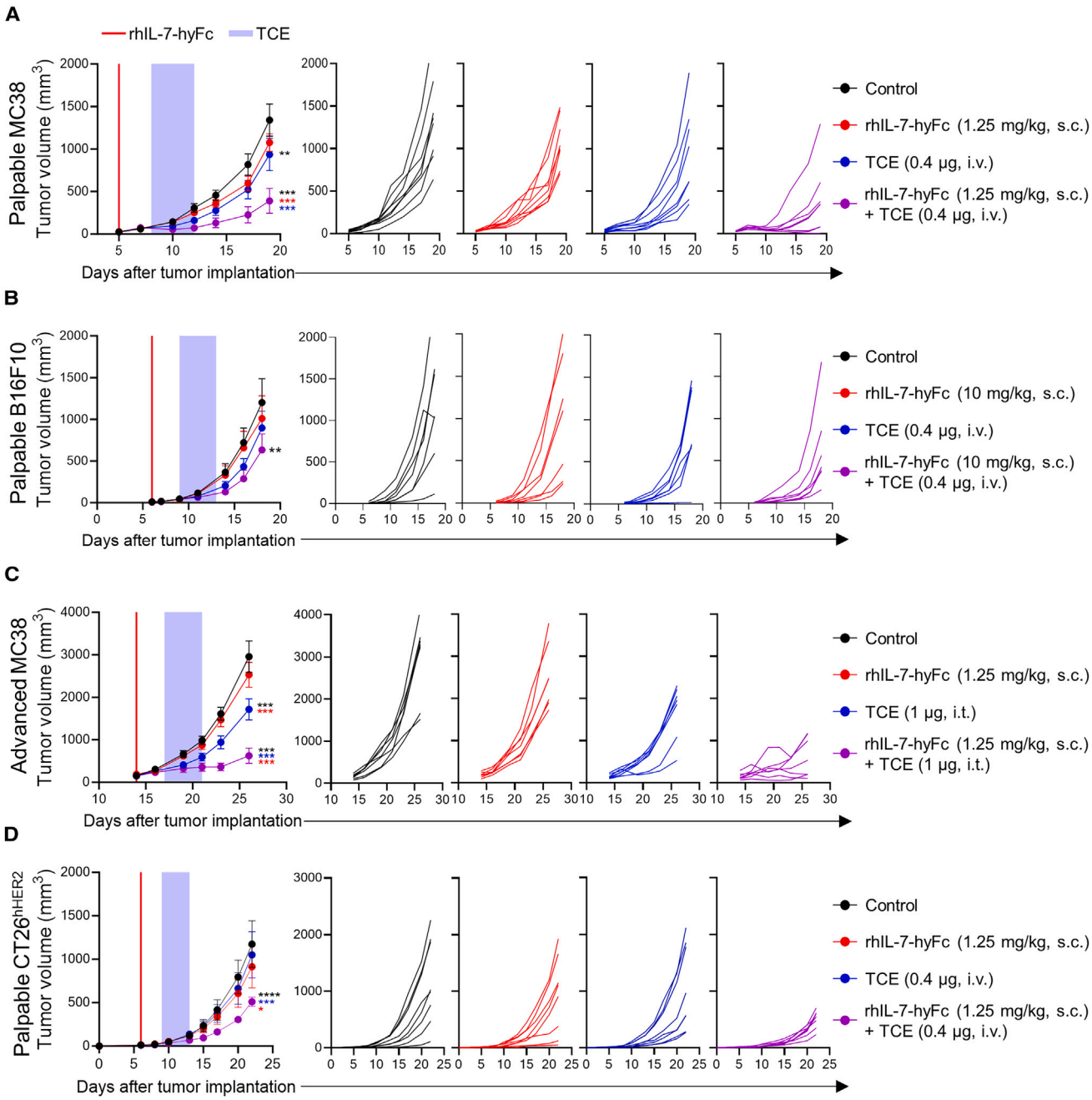

Figure 4. Combination therapy with rhIL-7-hyFc and TCE enhances antitumor responses

(A–D) Average (left) and individual (right) tumor growth after combination therapy in (A) palpable MC38, (B) palpable B16F10, (C) advanced MC38, and (D) palpable CT26^{hHER2} tumor models (n = 6–8 per group). Mice were s.c. treated with 1.25 mg kg^{-1} (A, C, and D) or 10 mg kg^{-1} (B) of rhIL-7-hyFc when the tumor was considered palpable (A, B, and D) or advanced (C). And then 0.4 μg of PD-L1×CD3 TCE (A and B), 1 μg of PD-L1×CD3 TCE (C), or 0.4 μg of HER2×CD3 TCE (D) was administered five times daily 3 days after rhIL-7-hyFc treatment. TCEs were injected intravenously (i.v.) for (A), (B), and (D) and i.t. for (C). The administration of rhIL-7-hyFc and TCE is indicated by red lines and blue columns, respectively. Data are shown as mean ± SEM and representative of two or three independent experiments. *p < 0.05, **p < 0.01, ***p < 0.001, and ****p < 0.0001 by two-way ANOVA and Tukey's multiple comparisons test. See also Figures S5 and S6.

TCE promotes cytotoxicity in rhIL-7-hyFc-induced bystander CD8 TILs

Next, we investigated the impact of rhIL-7-hyFc and TCE combination therapy on the immune cell composition within MC38 tumors, including CD8 TILs. Due to difficulties in recovering sufficient live leukocytes for flow cytometry-based analysis after the full regimen of TCE treatments, we chose to perform the TIL analysis at an earlier time point, following

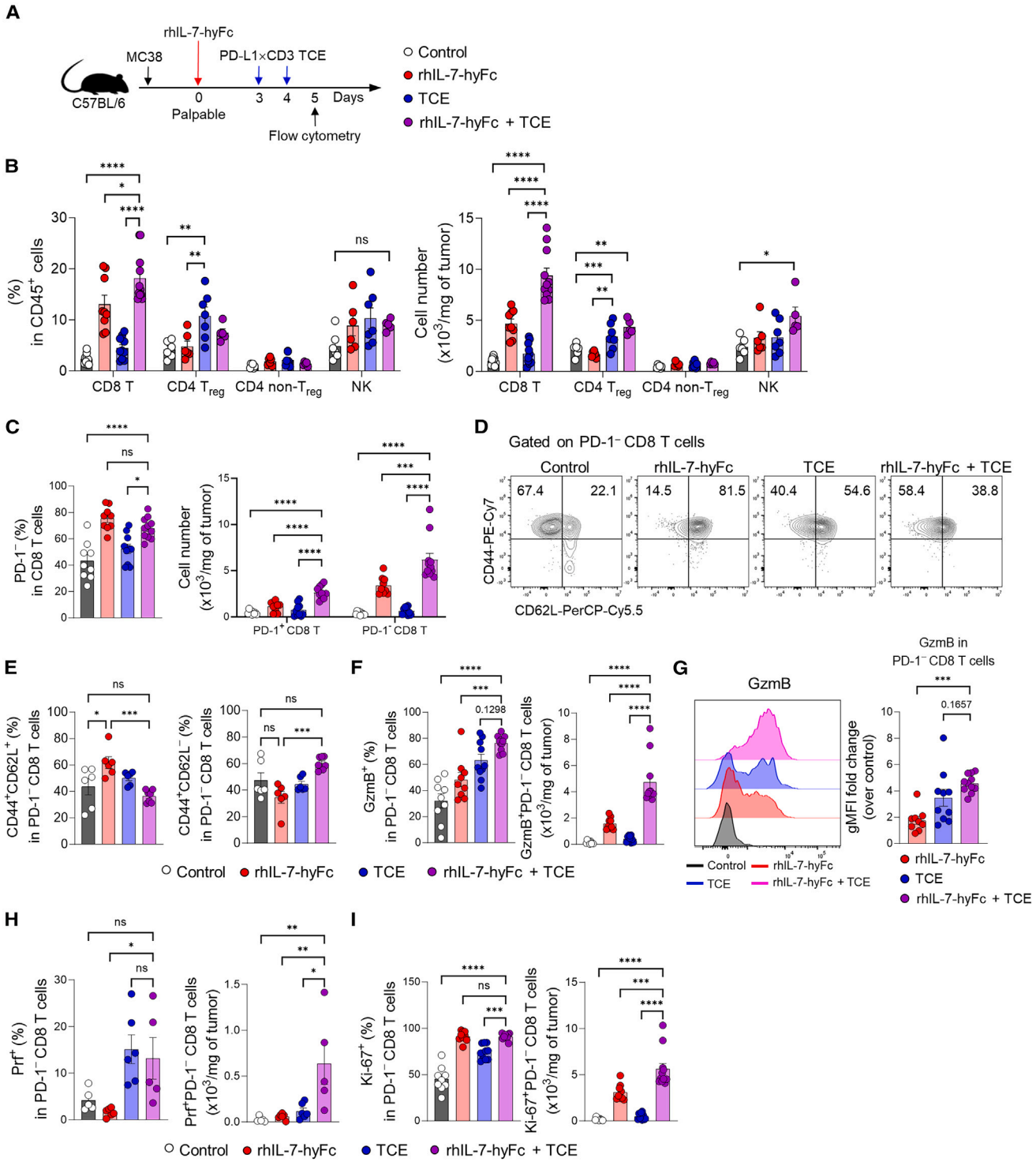

Figure 5. TCE combination promotes the cytotoxic activity of rhIL-7-hyFc-induced bystander CD8 TILs

(A) Experimental scheme. Mice bearing palpable MC38 tumors were injected s.c. with rhIL-7-hyFc (1.25 mg kg^{-1}). Three days after rhIL-7-hyFc treatment, mice were treated i.v. with PD-L1×CD3 TCE (0.4 μg) 2 times daily. Twenty-four hours after the last treatment, mice were analyzed for TILs (n = 4–6 per group).

(B) Frequencies (left) and numbers (right) of CD8 T, CD4 T_{reg}, CD4 non-T_{reg}, and NK cells.

(C) Frequencies of PD-1$^-$ cells (left) and numbers of PD-1$^+$ and PD-1$^-$ cells among the total CD8 T cells (right).

(D) Representative plots showing the expression of CD44 and CD62L in PD-1$^-$ CD8 T cells.

(E) Frequencies of CD44$^+$CD62L$^+$ (left) and CD44$^+$CD62L$^-$ (right) cells among PD-1$^-$ CD8 T cells.

(legend continued on next page)

two to three administrations of TCE (Figure 5A). The number of CD8 TILs increased dramatically with the combination therapy when compared with rhIL-7-hyFc or TCE monotherapy, although regulatory T (T_{reg}), CD4 non-T_{reg} cell, and NK cell counts were equivalent (Figure 5B). However, the numbers of $CD11b^+$ myeloid cells, including MDSCs and TAMs, were similarly reduced by monotherapies or combination therapy (Figure S7A). This reduction is primarily due to the suppression of myelopoiesis in the bone marrow induced by rhIL-7-hyFc, as demonstrated in our previous study.[36] Therefore, the ratio of CD8/T_{reg} or CD8/CD11b cells, which is employed as an immune environment indicator for TME, was elevated in rhIL-7-hyFc mono- and combination therapy (Figure S7B). These results suggest that rhIL-7-hyFc and TCE combination induces the typical inflamed TME by altering the immune cell composition of tumors to become immunostimulatory with a high number of CD8 T cells. The combination therapy significantly enhanced the numbers of both $PD\text{-}1^+$ tumor-reactive and $PD\text{-}1^-$ bystander cells, but the proportion of $PD\text{-}1^-$ cells was reduced compared with that of rhIL-7-hyFc monotherapy (Figure 5C).

We further addressed how the TCE combination changed the bystander CD8 TILs induced by rhIL-7-hyFc treatment. Interestingly, the majority of $PD\text{-}1^-$ CD8 TILs in rhIL-7-hyFc monotherapy showed $CD44^+CD62L^+$ CM T cell (T_{CM}) phenotype, but the TCE combination significantly increased the proportion of $CD44^+CD62L^-$ effector memory T cell (T_{EM}) phenotype cells (Figures 5D and 5E), suggesting the conversion of CD8 T cell phenotypes by TCE stimulation. Compared to monotherapies, rhIL-7-hyFc and TCE combination therapy increased the number of $GzmB^+$ cells in $PD\text{-}1^-$ CD8 TILs with substantially greater levels of GzmB expression (Figures 5F and 5G). The number of Prf^+ and $Ki\text{-}67^+$ $PD\text{-}1^-$ CD8 TILs was similarly raised by combination therapy (Figures 5H and 5I). On the other hand, $PD\text{-}1^+$ tumor-reactive cells, like the previous *ex vivo* results, have already saturated the expression of cytotoxic molecules in tumors, therefore, they did not show additional changes by mono- or combination therapy (Figures S7C–S7F). To validate the activation of $PD\text{-}1^-$ CD8 TILs across different tumor models following rhIL-7-hyFc and TCE combination therapy, we analyzed CD8 TILs in B16F10 and $CT26^{hHER2}$ tumors. Although some variations were observed between the models, in both, the combination therapy increased the expression of cytotoxic molecules such as GzmB and Prf in $PD\text{-}1^-$ bystander CD8 T cells, while not significantly affecting their expression in $PD\text{-}1^+$ tumor-reactive cells (Figures S8A–S8J). Taken together, these findings indicate that TCE combination with rhIL-7-hyFc has a more significant impact on bystander CD8 TILs than tumor-reactive cells. TCE treatment causes phenotypic alterations in rhIL-7-hyFc-induced $PD\text{-}1^-$ bystander CD8 TILs, which acquire cytotoxic function via TCE-mediated redirection.

TCE alters the transcriptome of bystander CD8 TILs inducing a distinct cell subset resembling tumor-reactive CD8 TILs

To further investigate the differentiation process of CD8 TILs induced by rhIL-7-hyFc and TCE combination therapy, we performed paired scRNA-seq and scTCR-seq analyses on CD8 TILs from palpable MC38 tumors following the therapy (Figure S9A). CD8 TILs were classified into 10 clusters (Figure 6A). Clusters 1, 2, and 7 were *Pdcd1*$^-$*Tcf7*$^+$ subsets strongly expressing naive/CM marker genes (*Sell, Ccr7, Lef1, Bcl2*) and grouped as bystander cells (Figures 6B–6D). In contrast, clusters 0, 4, 5, 6, and 9 were *Pdcd1*$^+$*Tcf7*$^-$ subsets expressing T cell differentiation/exhaustion markers (*Ctla4, Tnfrsf9, Havcr2, Tox, Prf1*) and grouped as tumor-reactive cells (Figures 6B–6D). Accordingly, the scTCR-seq analysis revealed that the top six CD8 clonotypes were found in the tumor-reactive cell subset (Figure 6E). Interestingly, we were able to identify clusters 3 and 8 with a distinct transcriptome pattern from the bystander and tumor-reactive subsets (Figure 6B), which were grouped as proliferating cell subsets with high expression of genes involved in cell cycle regulation (*Mcm3, Mcm7, Mki67, Ccna2, Cdc45*) (Figure 6C). The GO analysis terms of these clusters also included gene sets directly related to cell proliferation, such as DNA replication, chromosome organization, and cell cycle regulation (Figure S9B). When the differentiation trajectory was examined using pseudotime analysis, the path from bystander cells to tumor-reactive cells emerged, and clusters 3 and 8 were located between the two subsets (Figure S9C). These single-cell transcriptomic data and previous cell-based analysis results suggest that clusters 3 and 8 are transitional cell subsets in which rhIL-7-hyFc-induced bystander cells are TCR-stimulated by TCE combination. The fact that the TCE combination reduced bystander but increased transitional and tumor-reactive subsets when compared with rhIL-7-hyFc monotherapy supports our hypothesis (Figure 6B).

When analyzing DEGs of CD8 TIL subsets, the TCE combination produced more gene-expression changes in bystander and transitional subsets than tumor-reactive subset (Figures 6F and S9D). GO analysis showed that the TCE combination induced a significant increase in the NADH regeneration-related gene set in bystander cells (Figure 6G, top). In addition, TCE combination upregulated gene sets associated with T cell activation, glycolysis, and effector/cell motility in bystander cells while decreasing naive/CM-associated genes (Figures 6G and 6H). This suggests that metabolic reprogramming is followed by the activation and differentiation of bystander cells by TCE. In transitional cells, the TCE combination dramatically elevated the genes linked with cell activation and cytotoxicity (Figure 6G, middle). In particular, the expression of *Tcf7*, a memory cell marker, was completely downregulated, but the expression of cytotoxic molecules, such as *Gzma* and *Gzmb*, was obtained in transitional cells (Figure 6H), implying that they may be transformed into

(F, H, and I) Frequencies (left) and numbers (right) of $GzmB^+$ cells (F), Prf^+ cells (H), and $Ki\text{-}67^+$ cells (I) among $PD\text{-}1^-$ CD8 T cells.
(G) Histogram of GzmB expression in $PD\text{-}1^-$ CD8 T cells (left) and fold change of GzmB geometric mean fluorescence intensity (gMFI) compared with the buffer group in $PD\text{-}1^-$ CD8 T cells. Data are shown as mean ± SEM and summary of two independent experiments (B, C, F, G, and I) or representative of two independent experiments (E and H). $^*p < 0.05$, $^{**}p < 0.01$, $^{***}p < 0.001$, and $^{****}p < 0.0001$ by one-way ANOVA and Tukey's multiple comparisons test. ns, not significant. See also Figures S7 and S8.

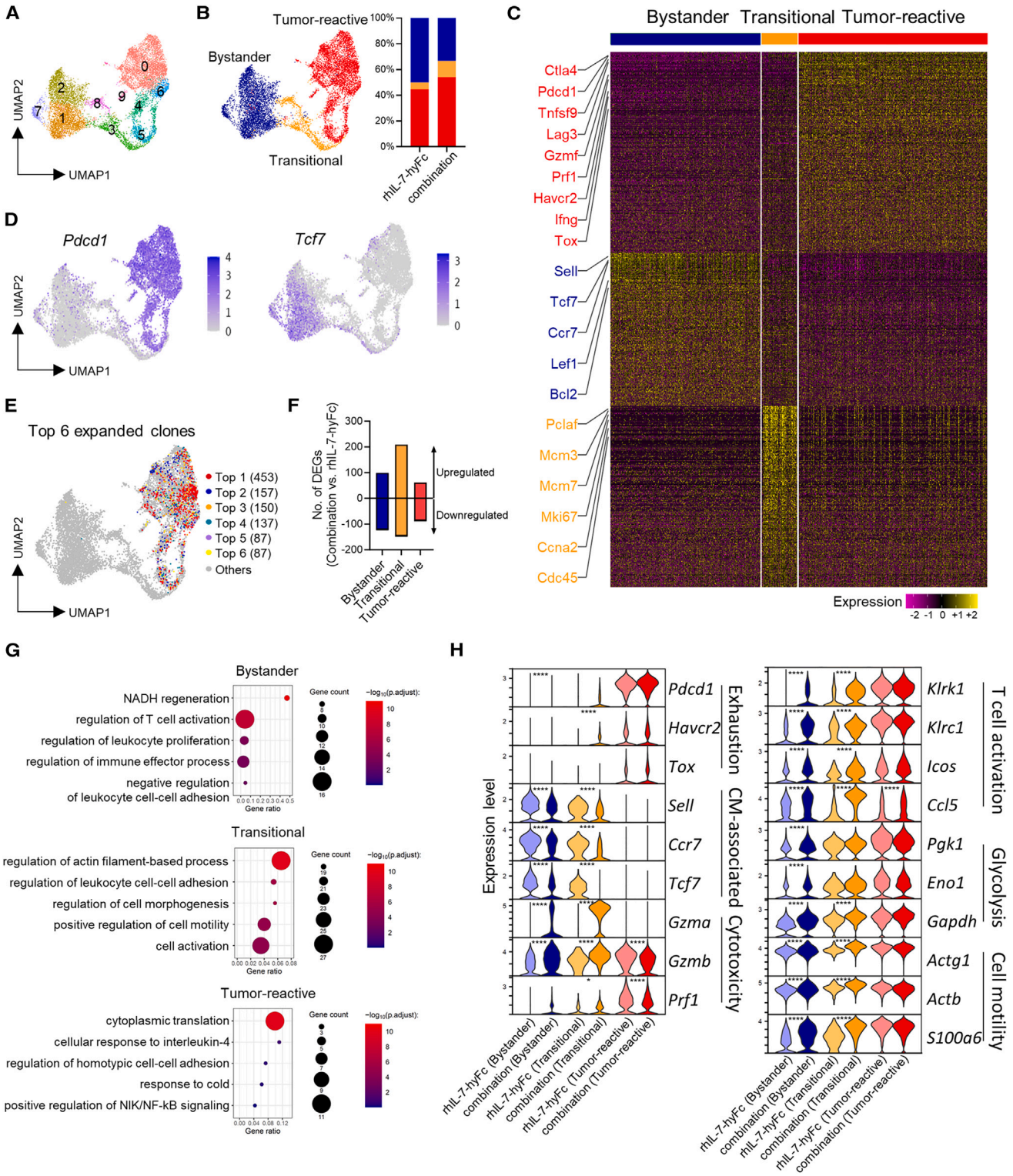

Figure 6. Transcriptome analysis of CD8 TIL subsets in combination therapy

scRNA-seq results of CD8 TILs from mice bearing MC38 tumors treated with rhIL-7-hyFc alone or a combination of rhIL-7-hyFc and TCE. C57BL/6 mice bearing palpable MC38 tumors were injected s.c. with rhIL-7-hyFc (1.25 mg kg^{-1}). Three days after rhIL-7-hyFc treatment, mice were treated i.v. with PD-L1×CD3 TCE (0.4 μg) three times daily. Tumors were collected 24 h after the last treatment. Collected tumor tissues were pooled for analysis (n = 12 rhIL-7-hyFc and n = 24 combination).

(legend continued on next page)

tumor-reactive cytotoxic cells by TCE redirection. TCE combination, like earlier studies, did not generate detectable transcriptomic changes in T cell activation and differentiation/exhaustion in tumor-reactive cells (Figure 6H). Flow cytometry analysis confirmed that PD-1$^-$ CD8 T cells, encompassing both bystander and transitional populations, exhibited a decrease in CM-associated molecule expression while simultaneously increasing their expression of cytotoxic molecules. In contrast, PD-1$^+$ tumor-reactive cells demonstrated minimal changes in the expression of these molecules (Figures S10A–S10D). Nevertheless, the increase in a gene set associated with cytoplasmic translation in GO analysis suggests that TCE can also regulate the activity of tumor-reactive cells (Figure 6G, bottom). In conclusion, our single-cell analysis reveals that T_{CM}-phenotype bystander CD8 TILs, which are increased in tumors by rhIL-7-hyFc administration, are further activated, proliferated, and differentiated into a distinct cell subset that obtains effector features by TCE redirection.

DISCUSSION

As the fact that numerous factors of solid cancer TME inhibit the efficacy of cancer immunotherapy including ICI has been accumulated, many strategies to overcome immunosuppressive TME environment through a combination of anticancer therapeutics have been proposed.[52–54] It is desirable to find the optimal combination regimen based on scientific rationale rather than a simple combination of modalities known to have anticancer effects alone. Through this study, we propose that the combination of Fc-fused IL-7, a T cell amplifier, and TCE, a T cell redirector, is the best combination partner to show improved antitumor efficacy by modifying CD8 T cell landscape in tumors.

IL-7, as a T cell homeostatic cytokine, plays a crucial role in regulating T cell development and quantity.[55] Many attempts to employ IL-7 as a biopharmaceutical have led to the development of rhIL-7-hyFc, whose anticancer activity and safety have been validated in recent preclinical and clinical investigations.[36,37,40,56,57] It is intuitive that rhIL-7-hyFc would synergize with T cell-focused therapeutic modalities, as it showed outstanding combination efficacy with ICIs and CAR T therapy, which are gold standards of cancer immunotherapy.[36,56] However, how rhIL-7-hyFc therapy affects the development and function of CD8 T cell subsets in tumors has not been thoroughly investigated.

T cell lymphopenia causes an increase in the blood concentration of IL-7, which causes homeostatic T cell proliferation to compensate for the shortage of T cells.[58,59] Exogenous administration of rhIL-7-hyFc, on the other hand, can induce CD8 T cell amplification in the T cell replete condition, and expanded CD8 T cells acquire T_{CM}-phenotype and tumor tropism with CXCR3 and CCR5 upregulation.[36] Consequently, the number of CD8 T cells in tumors increases rapidly following rhIL-7-hyFc treatment, although the majority of them are naturally polyclonal bystander T cells. Our single-cell transcriptome analysis clearly demonstrated the bystander features of rhIL-7-hyFc-induced PD-1$^-$ CD8 TILs that have limited tumor responsiveness on their own. However, we noticed that those bystander CD8 TILs exhibit enhanced TCR-responsiveness and potent recall proliferative potential. Therefore, bispecific TCEs may be an ideal modality for mobilizing bystander cells for antitumor response. TCEs were able to elicit cytotoxicity of bystander CD8 TILs when recognizing tumor antigens such as PD-L1 and HER2. Transcriptome analysis revealed that TCE-redirected bystander cells lose the CM-phenotype and differentiate into cycling transitional cells that obtain cytotoxic molecules via metabolic reprogramming. Consequently, in the context of TCE immunotherapy, two types of tumor-targeting cytotoxic T lymphocytes (CTLs) are present within the tumor: one is the naturally occurring tumor-reactive CD8 T cell, which is primed by tumor antigen presentation in the tumor-draining lymph node and then migrates to the tumor, and the other is the redirected bystander CD8 T cell, which acquires induced tumor reactivity through TCE. Determining the extent to which TCE-stimulated bystander T cells directly contribute to tumor clearance is challenging. However, the adoptive transfer experiment conducted in RAG1$^{-/-}$ mice, by specifically focusing on TCE-redirected bystander cells, demonstrates that these cells can exhibit sufficient antitumor capabilities. This suggests that under normal conditions and given adequate numbers and functionality, they indeed possess significant antitumor potential.

In contrast, tumor-reactive CD8 TILs were not the primary target of TCE immunotherapy since TCE did not cause noticeable changes in the transcriptome and effector protein expression in tumor-reactive cells. Because tumor-reactive cells are already receiving TCR signals from tumor antigens, the effect of additional TCE-induced activation may be minimal. Alternatively, TCE stimulation may not be sufficient to reinvigorate tumor-reactive CD8 TILs that have experienced T cell exhaustion. In this respect, the recent anti-BCMA×anti-CD3 TCE immunotherapy study in MM patients is interesting, showing that pre-existing naive/memory CD8 T cells were transformed into effector-phenotype cells by TCE redirection and were associated with a favorable clinical response.[17] The anti-BCMA×anti-CD3 TCE, on the other hand, had no significant effect on exhausted CD8 T cells. Therefore, those results revealed that the composition of pre-existing CD8 T cells in MM patients determines the clinical

(A) UMAP plot showing each CD8 TIL cluster.
(B) Supervised clustering of CD8 TILs according to gene-expression characteristics (left) and bar graph depicting the proportion of three CD8 TIL subclusters in each treatment condition (right).
(C) Heatmap showing the DEGs between supervised groups.
(D) Featured plots showing the expression of *Pdcd1* (left) and *Tcf7* (right) genes.
(E) UMAP plot of top six most expanded clones.
(F) Number of DEGs in each supervised CD8 TIL subcluster from mice with combination therapy compared with the rhIL-7-hyFc-treated group.
(G) Dot plots of GO enrichment analysis of upregulated DEGs by combination therapy in each CD8 TIL subcluster.
(H) Violin plots showing the expression of genes related to exhaustion, CM-associated, cytotoxicity, T cell activation, glycolysis, and cell motility. See also Figures S9 and S10; Table S3.

response of TCE immunotherapy.[17] Our findings also suggest that the composition of CD8 TILs in solid tumors will be a determining factor for the efficacy of TCE immunotherapy; if TME contains a large number of "TCE-sensitive" CD8 TILs that are non-exhausted but have high recall capacity, we can expect a robust antitumor response. As a result, rhIL-7-hyFc can be an ideal partner in optimizing the efficacy of TCE immunotherapy since it can substantially increase TCE-sensitive T_{CM}-phenotype bystander CD8 TILs across various tumor types.

Many bispecific TCEs are now being explored for anticancer immunotherapy. However, applying TCEs to solid cancers remains a major challenge.[60] Our findings indicate that the success of TCE immunotherapy is dependent on the quantity, function, and subset composition of CD8 T cells in solid tumors, and we propose rhIL-7-hyFc as a therapeutic agent capable of promoting such a TCE-sensitive TME.

Limitations of the study

Our study presents several limitations that merit detailed examination and discussion. Primarily, while our *in vitro* assays and adoptive transfer experiments in RAG1$^{-/-}$ mice suggest tumoricidal activity of bystander CD8 TILs upon TCE stimulation, the exact magnitude of their contribution to the efficacy of rhIL-7-hyFc and TCE combination therapy remains to be fully determined. Moreover, considering that TCE efficacy can extend beyond CD8 T cells to other CD3^{+} T cell subsets, including CD4 T cells, our findings necessitate careful interpretation, reflecting the complex interplay within the T cell compartment. The potential modulation of the myeloid cell landscape within the TME by rhIL-7-hyFc, through regulation of hematopoiesis,[36,61] adds another layer of complexity to our results. Thus, a more comprehensive analysis with a single-cell level examination of the immune cell composition post-therapy is crucial for a detailed understanding. Future studies exploring the synergy between rhIL-7-hyFc/TCE therapy and other anticancer modalities, especially ICIs, are imperative to delineate combinatory treatment strategies. Crucially, translating our findings to clinical settings requires thorough validation in human studies to determine if the observed increase in bystander CD8 TILs by rhIL-7-hyFc monotherapy exhibits comparable antitumor activities in human cancers.

STAR★METHODS

Detailed methods are provided in the online version of this paper and include the following:

SUPPLEMENTAL INFORMATION

Supplemental information can be found online at https://doi.org/10.1016/j.xcrm.2024.101567.

ACKNOWLEDGMENTS

We are grateful to Tae Won Kim at Asan Medical Center (Republic of Korea) and Myung Ah Lee at Seoul St, Mary's Hospital (Republic of Korea) for providing human samples. This research was supported by the Korea Drug Development Fund funded by Ministry of Science and ICT (MSIT), Ministry of Trade, Industry, and Energy, and Ministry of Health and Welfare (RS-2023-00258678), the National Research Foundation (NRF) funded by the Korean government (MSIT: RS-2023-00225255, RS-2023-00221112, 2020R1A5A8019180, and 2019R1A2C1002350), the BK21 program (4120200313623) funded by the Ministry of Education, and by Research Institute of NeoImmuneTech, Inc.

AUTHOR CONTRIBUTIONS

Conceptualization: K.-J.L., N.T., D.C., D.H.K., and S.-W.L. Methodology: K.-J.L., D.C., N.T., H.W.S., Y.-W.K., D.M., Y.O., S.P., J.-H.K., S.J., J.Y., U.P., D.H.H., M.-S.B., S.-H.P., J.S., M.L., S.-K.I., Y.P., S.S.C., D.H.K., and S.-W.L. Investigation: K.-J.L., N.T., H.W.S., S.P., Y.-W.K., D.M., Y.O., and J.-H.K. Visualization: K.-J.L., H.W.S., D.H.H., and M.-S.B. Funding acquisition: D.C., S.S.C., D.H.K., and S.-W.L. Project administration: D.C., J.S., S.S.C., D.H.K., and S.-W.L. Supervision: S.S.C., D.H.K., and S.-W.L. Writing – original draft: K.-J.L., N.T., and H.W.S. Writing – review & editing: D.C., Y.P., S.S.C., D.H.K., S.-W.L.

DECLARATION OF INTERESTS

M.L., S.-K.I., and D.C. are employees of the Research Institute of NeoImmuneTech, Inc., which supports the supply of rhIL-7-hyFc and its formulation buffer.

Received: September 3, 2023
Revised: February 29, 2024
Accepted: April 19, 2024
Published: May 13, 2024

REFERENCES

1. Raskov, H., Orhan, A., Christensen, J.P., and Gögenur, I. (2021). Cytotoxic CD8(+) T cells in cancer and cancer immunotherapy. Br. J. Cancer *124*, 359–367. https://doi.org/10.1038/s41416-020-01048-4.
2. Chen, D.S., and Mellman, I. (2013). Oncology meets immunology: the cancer-immunity cycle. Immunity *39*, 1–10. https://doi.org/10.1016/j.immuni.2013.07.012.
3. Ribas, A., and Wolchok, J.D. (2018). Cancer immunotherapy using checkpoint blockade. Science *359*, 1350–1355. https://doi.org/10.1126/science.aar4060.
4. Larkin, J., Chiarion-Sileni, V., Gonzalez, R., Grob, J.J., Rutkowski, P., Lao, C.D., Cowey, C.L., Schadendorf, D., Wagstaff, J., Dummer, R., et al. (2019). Five-Year Survival with Combined Nivolumab and Ipilimumab in

Advanced Melanoma. N. Engl. J. Med. *381*, 1535–1546. https://doi.org/10.1056/NEJMoa1910836.

5. Chowell, D., Morris, L.G.T., Grigg, C.M., Weber, J.K., Samstein, R.M., Makarov, V., Kuo, F., Kendall, S.M., Requena, D., Riaz, N., et al. (2018). Patient HLA class I genotype influences cancer response to checkpoint blockade immunotherapy. Science *359*, 582–587. https://doi.org/10.1126/science.aao4572.
6. Sharma, P., Hu-Lieskovan, S., Wargo, J.A., and Ribas, A. (2017). Primary, Adaptive, and Acquired Resistance to Cancer Immunotherapy. Cell *168*, 707–723. https://doi.org/10.1016/j.cell.2017.01.017.
7. Huehls, A.M., Coupet, T.A., and Sentman, C.L. (2015). Bispecific T-cell engagers for cancer immunotherapy. Immunol. Cell Biol. *93*, 290–296. https://doi.org/10.1038/icb.2014.93.
8. Messaoudene, M., Mourikis, T.P., Michels, J., Fu, Y., Bonvalet, M., Lacroix-Trikki, M., Routy, B., Fluckiger, A., Rusakiewicz, S., Roberti, M.P., et al. (2019). T-cell bispecific antibodies in node-positive breast cancer: novel therapeutic avenue for MHC class I loss variants. Ann. Oncol. *30*, 934–944. https://doi.org/10.1093/annonc/mdz112.
9. Bachireddy, P., Burkhardt, U.E., Rajasagi, M., and Wu, C.J. (2015). Hematological malignancies: at the forefront of immunotherapeutic innovation. Nat. Rev. Cancer *15*, 201–215. https://doi.org/10.1038/nrc3907.
10. Przepiorka, D., Ko, C.W., Deisseroth, A., Yancey, C.L., Candau-Chacon, R., Chiu, H.J., Gehrke, B.J., Gomez-Broughton, C., Kane, R.C., Kirshner, S., et al. (2015). FDA Approval: Blinatumomab. Clin. Cancer Res. *21*, 4035–4039. https://doi.org/10.1158/1078-0432.CCR-15-0612.
11. Kang, C. (2022). Teclistamab: First Approval. Drugs *82*, 1613–1619. https://doi.org/10.1007/s40265-022-01793-1.
12. Montazeri, K., Pattanayak, V., and Sullivan, R.J. (2023). Tebentafusp in the Treatment of Metastatic Uveal Melanoma: Patient Selection and Special Considerations. Drug Des. Devel. Ther. *17*, 333–339. https://doi.org/10.2147/dddt.s368954.
13. Braig, F., Brandt, A., Goebeler, M., Tony, H.-P., Kurze, A.-K., Nollau, P., Bumm, T., Böttcher, S., Bargou, R.C., and Binder, M. (2017). Resistance to anti-CD19/CD3 BiTE in acute lymphoblastic leukemia may be mediated by disrupted CD19 membrane trafficking. Blood *129*, 100–104. https://doi.org/10.1182/blood-2016-05-718395.
14. Cosenza, M., Sacchi, S., and Pozzi, S. (2021). Cytokine Release Syndrome Associated with T-Cell-Based Therapies for Hematological Malignancies: Pathophysiology, Clinical Presentation, and Treatment. Int. J. Mol. Sci. *22*, 7652. https://doi.org/10.3390/ijms22147652.
15. Singh, A., Dees, S., and Grewal, I.S. (2021). Overcoming the challenges associated with CD3+ T-cell redirection in cancer. Br. J. Cancer *124*, 1037–1048. https://doi.org/10.1038/s41416-020-01225-5.
16. Ströhlein, M.A., Lefering, R., Bulian, D.R., and Heiss, M.M. (2014). Relative lymphocyte count is a prognostic parameter in cancer patients with catumaxomab immunotherapy. Med. Hypotheses *82*, 295–299. https://doi.org/10.1016/j.mehy.2013.12.014.
17. Friedrich, M.J., Neri, P., Kehl, N., Michel, J., Steiger, S., Kilian, M., Leblay, N., Maity, R., Sankowski, R., Lee, H., et al. (2023). The pre-existing T cell landscape determines the response to bispecific T cell engagers in multiple myeloma patients. Cancer Cell *41*, 711–725.e6. https://doi.org/10.1016/j.ccell.2023.02.008.
18. Slaney, C.Y., Wang, P., Darcy, P.K., and Kershaw, M.H. (2018). CARs versus BiTEs: A Comparison between T Cell–Redirection Strategies for Cancer Treatment. Cancer Discov. *8*, 924–934. https://doi.org/10.1158/2159-8290.cd-18-0297.
19. Arvedson, T., Bailis, J.M., Britten, C.D., Klinger, M., Nagorsen, D., Coxon, A., Egen, J.G., and Martin, F. (2022). Targeting Solid Tumors with Bispecific T Cell Engager Immune Therapy. Annu. Rev. Cancer Biol. *6*, 17–34. https://doi.org/10.1146/annurev-cancerbio-070620-104325.
20. Simoni, Y., Becht, E., Fehlings, M., Loh, C.Y., Koo, S.L., Teng, K.W.W., Yeong, J.P.S., Nahar, R., Zhang, T., Kared, H., et al. (2018). Bystander CD8(+) T cells are abundant and phenotypically distinct in human tumour infiltrates. Nature *557*, 575–579. https://doi.org/10.1038/s41586-018-0130-2.
21. Meier, S.L., Satpathy, A.T., and Wells, D.K. (2022). Bystander T cells in cancer immunology and therapy. Nat. Cancer *3*, 143–155. https://doi.org/10.1038/s43018-022-00335-8.
22. Dangaj, D., Bruand, M., Grimm, A.J., Ronet, C., Barras, D., Duttagupta, P.A., Lanitis, E., Duraiswamy, J., Tanyi, J.L., Benencia, F., et al. (2019). Cooperation between Constitutive and Inducible Chemokines Enables T Cell Engraftment and Immune Attack in Solid Tumors. Cancer Cell *35*, 885–900.e10. https://doi.org/10.1016/j.ccell.2019.05.004.
23. Maurice, N.J., McElrath, M.J., Andersen-Nissen, E., Frahm, N., and Prlic, M. (2019). CXCR3 enables recruitment and site-specific bystander activation of memory CD8+ T cells. Nat. Commun. *10*, 4987. https://doi.org/10.1038/s41467-019-12980-2.
24. Li, H., Van Der Leun, A.M., Yofe, I., Lubling, Y., Gelbard-Solodkin, D., Van Akkooi, A.C.J., Van Den Braber, M., Rozeman, E.A., Haanen, J.B.A.G., Blank, C.U., et al. (2019). Dysfunctional CD8 T Cells Form a Proliferative, Dynamically Regulated Compartment within Human Melanoma. Cell *176*, 775–789.e18. https://doi.org/10.1016/j.cell.2018.11.043.
25. Caushi, J.X., Zhang, J., Ji, Z., Vaghasia, A., Zhang, B., Hsiue, E.H.C., Mog, B.J., Hou, W., Justesen, S., Blosser, R., et al. (2021). Transcriptional programs of neoantigen-specific TIL in anti-PD-1-treated lung cancers. Nature *596*, 126–132. https://doi.org/10.1038/s41586-021-03752-4.
26. Oliveira, G., Stromhaug, K., Klaeger, S., Kula, T., Frederick, D.T., Le, P.M., Forman, J., Huang, T., Li, S., Zhang, W., et al. (2021). Phenotype, specificity and avidity of antitumour CD8(+) T cells in melanoma. Nature *596*, 119–125. https://doi.org/10.1038/s41586-021-03704-y.
27. Mognol, G.P., Spreafico, R., Wong, V., Scott-Browne, J.P., Togher, S., Hoffmann, A., Hogan, P.G., Rao, A., and Trifari, S. (2017). Exhaustion-associated regulatory regions in CD8(+) tumor-infiltrating T cells. Proc. Natl. Acad. Sci. USA *114*, E2776–E2785. https://doi.org/10.1073/pnas.1620498114.
28. Sullivan, P.M., Reed, S.J., Kalia, V., and Sarkar, S. (2021). Solid Tumor Microenvironment Can Harbor and Support Functional Properties of Memory T Cells. Front. Immunol. *12*, 706150. https://doi.org/10.3389/fimmu.2021.706150.
29. Rosato, P.C., Wijeyesinghe, S., Stolley, J.M., Nelson, C.E., Davis, R.L., Manlove, L.S., Pennell, C.A., Blazar, B.R., Chen, C.C., Geller, M.A., et al. (2019). Virus-specific memory T cells populate tumors and can be repurposed for tumor immunotherapy. Nat. Commun. *10*, 567. https://doi.org/10.1038/s41467-019-08534-1.
30. Millar, D.G., Ramjiawan, R.R., Kawaguchi, K., Gupta, N., Chen, J., Zhang, S., Nojiri, T., Ho, W.W., Aoki, S., Jung, K., et al. (2020). Antibody-mediated delivery of viral epitopes to tumors harnesses CMV-specific T cells for cancer therapy. Nat. Biotechnol. *38*, 420–425. https://doi.org/10.1038/s41587-019-0404-8.
31. Chaganty, B.K.R., Qiu, S., Lu, Y., Lopez-Berestein, G., Ozpolat, B., and Fan, Z. (2022). Redirecting host preexisting influenza A virus immunity for cancer immunotherapy. Cancer Immunol. Immunother. *71*, 1611–1623. https://doi.org/10.1007/s00262-021-03099-9.
32. Gao, J., Zhao, L., Wan, Y.Y., and Zhu, B. (2015). Mechanism of Action of IL-7 and Its Potential Applications and Limitations in Cancer Immunotherapy. Int. J. Mol. Sci. *16*, 10267–10280. https://doi.org/10.3390/ijms160510267.
33. Kim, J.-H., Lee, K.-J., and Lee, S.-W. (2021). Cancer immunotherapy with T-cell targeting cytokines: IL-2 and IL-7. BMB Rep. *54*, 21–30. https://doi.org/10.5483/bmbrep.2021.54.1.257.
34. Park, J.H., Lee, S.W., Choi, D., Lee, C., and Sung, Y.C. (2024). Harnessing the Power of IL-7 to Boost T Cell Immunity in Experimental and Clinical Immunotherapies. Immune Netw. *24*, e9. https://doi.org/10.4110/in.2024.24.e9.
35. Nam, H.J., Song, M.Y., Choi, D.H., Yang, S.H., Jin, H.T., and Sung, Y.C. (2010). Marked enhancement of antigen-specific T-cell responses by

IL-7-fused nonlytic, but not lytic, Fc as a genetic adjuvant. Eur. J. Immunol. *40*, 351–358. https://doi.org/10.1002/eji.200939271.

36. Kim, J.H., Kim, Y.M., Choi, D., Jo, S.B., Park, H.W., Hong, S.W., Park, S., Kim, S., Moon, S., You, G., et al. (2020). Hybrid Fc-fused interleukin-7 induces an inflamed tumor microenvironment and improves the efficacy of cancer immunotherapy. Clin. Transl. Immunology *9*, e1168. https://doi.org/10.1002/cti2.1168.
37. Campian, J.L., Ghosh, S., Kapoor, V., Yan, R., Thotala, S., Jash, A., Hu, T., Mahadevan, A., Rifai, K., Page, L., et al. (2022). Long-Acting Recombinant Human Interleukin-7, NT-I7, Increases Cytotoxic CD8 T Cells and Enhances Survival in Mouse Glioma Models. Clin. Cancer Res. *28*, 1229–1239. https://doi.org/10.1158/1078-0432.CCR-21-0947.
38. Gros, A., Robbins, P.F., Yao, X., Li, Y.F., Turcotte, S., Tran, E., Wunderlich, J.R., Mixon, A., Farid, S., Dudley, M.E., et al. (2014). PD-1 identifies the patient-specific CD8(+) tumor-reactive repertoire infiltrating human tumors. J. Clin. Invest. *124*, 2246–2259. https://doi.org/10.1172/JCI73639.
39. Kim, G.M., Kim, S., Lee, M.A., Byun, M.-S., Choi, D., Yang, S.H., Woo, J.W., Sung, Y.C., Shin, E.-C., Park, S.-H., et al. (2024). GX-I7(rhIL-7-hyFc, efineptakin alfa), a long-acting IL-7, safely and effectively increased peripheral CD8+and CD4+T cells and TILs in patients with solid tumors. medRxiv. https://doi.org/10.1101/2024.02.12.23299638.
40. Kim, S., Lee, S.W., Koh, J.Y., Choi, D., Heo, M., Chung, J.Y., Lee, B.H., Yang, S.H., Sung, Y.C., Lee, H., et al. (2022). A single administration of hIL-7-hyFc induces long-lasting T-cell expansion with maintained effector functions. Blood Adv. *6*, 6093–6107. https://doi.org/10.1182/bloodadvances.2021006591.
41. Pasetto, A., Gros, A., Robbins, P.F., Deniger, D.C., Prickett, T.D., Matus-Nicodemos, R., Douek, D.C., Howie, B., Robins, H., Parkhurst, M.R., et al. (2016). Tumor- and Neoantigen-Reactive T-cell Receptors Can Be Identified Based on Their Frequency in Fresh Tumor. Cancer Immunol. Res. *4*, 734–743. https://doi.org/10.1158/2326-6066.cir-16-0001.
42. Scheper, W., Kelderman, S., Fanchi, L.F., Linnemann, C., Bendle, G., De Rooij, M.A.J., Hirt, C., Mezzadra, R., Slagter, M., Dijkstra, K., et al. (2019). Low and variable tumor reactivity of the intratumoral TCR repertoire in human cancers. Nat. Med. *25*, 89–94. https://doi.org/10.1038/s41591-018-0266-5.
43. Schurich, A., Kennedy, P.T., Nastouli, E., Gilson, R., Pallett, L.J., Jajbhay, D., Wijngaarden, J., Otano, I., Gill, U.S., Hansi, N., et al. (2016). Distinct Metabolic Requirements of Exhausted and Functional Virus-Specific CD8 T Cells in the Same Host. Cell Rep. *16*, 1243–1252. https://doi.org/10.1016/j.celrep.2016.06.078.
44. Wu, H., Zhao, X., Hochrein, S.M., Eckstein, M., Gubert, G.F., Knöpper, K., Mansilla, A.M., Öner, A., Doucet-Ladevèze, R., Schmitz, W., et al. (2023). Mitochondrial dysfunction promotes the transition of precursor to terminally exhausted T cells through HIF-1α-mediated glycolytic reprogramming. Nat. Commun. *14*, 6858. https://doi.org/10.1038/s41467-023-42634-3.
45. Li, F., Liu, H., Zhang, D., Ma, Y., and Zhu, B. (2022). Metabolic plasticity and regulation of T cell exhaustion. Immunology *167*, 482–494. https://doi.org/10.1111/imm.13575.
46. Wolf, T., Jin, W., Zoppi, G., Vogel, I.A., Akhmedov, M., Bleck, C.K.E., Beltraminelli, T., Rieckmann, J.C., Ramirez, N.J., Benevento, M., et al. (2020). Dynamics in protein translation sustaining T cell preparedness. Nat. Immunol. *21*, 927–937. https://doi.org/10.1038/s41590-020-0714-5.
47. Le Saout, C., Luckey, M.A., Villarino, A.V., Smith, M., Hasley, R.B., Myers, T.G., Imamichi, H., Park, J.H., O'Shea, J.J., Lane, H.C., and Catalfamo, M. (2017). IL-7-dependent STAT1 activation limits homeostatic CD4+ T cell expansion. JCI Insight *2*, e96228. https://doi.org/10.1172/jci.insight.96228.
48. Brinkmann, V., Cyster, J.G., and Hla, T. (2004). FTY720: Sphingosine 1-Phosphate Receptor-1 in the Control of Lymphocyte Egress and Endothelial Barrier Function. Am. J. Transplant. *4*, 1019–1025. https://doi.org/10.1111/j.1600-6143.2004.00476.x.
49. Kythreotou, A., Siddique, A., Mauri, F.A., Bower, M., and Pinato, D.J. (2018). Pd-L1. J. Clin. Pathol. *71*, 189–194. https://doi.org/10.1136/jclinpath-2017-204853.
50. Tang, H., Liang, Y., Anders, R.A., Taube, J.M., Qiu, X., Mulgaonkar, A., Liu, X., Harrington, S.M., Guo, J., Xin, Y., et al. (2018). PD-L1 on host cells is essential for PD-L1 blockade–mediated tumor regression. J. Clin. Invest. *128*, 580–588. https://doi.org/10.1172/jci96061.
51. Liu, L., Chen, J., Bae, J., Li, H., Sun, Z., Moore, C., Hsu, E., Han, C., Qiao, J., and Fu, Y.-X. (2021). Rejuvenation of tumour-specific T cells through bispecific antibodies targeting PD-L1 on dendritic cells. Nat. Biomed. Eng. *5*, 1261–1273. https://doi.org/10.1038/s41551-021-00800-2.
52. Murciano-Goroff, Y.R., Warner, A.B., and Wolchok, J.D. (2020). The future of cancer immunotherapy: microenvironment-targeting combinations. Cell Res. *30*, 507–519. https://doi.org/10.1038/s41422-020-0337-2.
53. Zhu, S., Zhang, T., Zheng, L., Liu, H., Song, W., Liu, D., Li, Z., and Pan, C.-X. (2021). Combination strategies to maximize the benefits of cancer immunotherapy. J. Hematol. Oncol. *14*, 156. https://doi.org/10.1186/s13045-021-01164-5.
54. Boshuizen, J., and Peeper, D.S. (2020). Rational Cancer Treatment Combinations: An Urgent Clinical Need. Mol. Cell *78*, 1002–1018. https://doi.org/10.1016/j.molcel.2020.05.031.
55. Mackall, C.L., Fry, T.J., and Gress, R.E. (2011). Harnessing the biology of IL-7 for therapeutic application. Nat. Rev. Immunol. *11*, 330–342. https://doi.org/10.1038/nri2970.
56. Kim, M.Y., Jayasinghe, R., Devenport, J.M., Ritchey, J.K., Rettig, M.P., O'Neal, J., Staser, K.W., Kennerly, K.M., Carter, A.J., Gao, F., et al. (2022). A long-acting interleukin-7, rhIL-7-hyFc, enhances CAR T cell expansion, persistence, and anti-tumor activity. Nat. Commun. *13*, 3296. https://doi.org/10.1038/s41467-022-30860-0.
57. Lee, S.W., Choi, D., Heo, M., Shin, E.C., Park, S.H., Kim, S.J., Oh, Y.K., Lee, B.H., Yang, S.H., Sung, Y.C., and Lee, H. (2020). hIL-7-hyFc, A Long-Acting IL-7, Increased Absolute Lymphocyte Count in Healthy Subjects. Clin. Transl. Sci. *13*, 1161–1169. https://doi.org/10.1111/cts.12800.
58. Ponchel, F., Cuthbert, R.J., and Goëb, V. (2011). IL-7 and lymphopenia. Clin. Chim. Acta *412*, 7–16. https://doi.org/10.1016/j.cca.2010.09.002.
59. Surh, C.D., and Sprent, J. (2008). Homeostasis of naive and memory T cells. Immunity *29*, 848–862. https://doi.org/10.1016/j.immuni.2008.11.002.
60. Moon, D., Tae, N., Park, Y., Lee, S.-W., and Kim, D.H. (2022). Development of Bispecific Antibody for Cancer Immunotherapy: Focus on T Cell Engaging Antibody. Immune Netw. *22*, e4. https://doi.org/10.4110/in.2022.22.e4.
61. Kim, S., Kim, Y.-M., Kim, H., Kang, Y.-W., Park, S., Yang, S.-I., Choi, D., Sung, Y.C., and Lee, S.-W. (2021). Fc-fused IL-7 mobilizes long-term HSCs in a pro-B cell-dependent manner and synergizes with G-CSF and AMD3100. Leukemia *35*, 3030–3034. https://doi.org/10.1038/s41375-021-01274-6.
62. Dong, H., Zhu, G., Tamada, K., Flies, D.B., Van Deursen, J.M.A., and Chen, L. (2004). B7-H1 Determines Accumulation and Deletion of Intrahepatic CD8+ T Lymphocytes. Immunity *20*, 327–336. https://doi.org/10.1016/s1074-7613(04)00050-0.
63. Penichet, M.L., Challita, P.M., Shin, S.U., Sampogna, S.L., Rosenblatt, J.D., and Morrison, S.L. (1999). In vivo properties of three human HER2/neu-expressing murine cell lines in immunocompetent mice. Lab. Anim. Sci. *49*, 179–188.
64. Choi, J.R., Kim, M.J., Tae, N., Wi, T.M., Kim, S.H., Lee, E.S., and Kim, D.H. (2020). BLI-Based Functional Assay in Phage Display Benefits the Development of a PD-L1-Targeting Therapeutic Antibody. Viruses *12*, 684. https://doi.org/10.3390/v12060684.
65. Carter, P., Presta, L., Gorman, C.M., Ridgway, J.B., Henner, D., Wong, W.L., Rowland, A.M., Kotts, C., Carver, M.E., and Shepard, H.M. (1992). Humanization of an anti-p185HER2 antibody for human cancer therapy.

Proc. Natl. Acad. Sci. USA *89*, 4285–4289. https://doi.org/10.1073/pnas.89.10.4285.

66. Alegre, M.L., Tso, J.Y., Sattar, H.A., Smith, J., Desalle, F., Cole, M., and Bluestone, J.A. (1995). An anti-murine CD3 monoclonal antibody with a low affinity for Fc gamma receptors suppresses transplantation responses while minimizing acute toxicity and immunogenicity. J. Immunol. *155*, 1544–1555.

67. Zheng, G.X.Y., Terry, J.M., Belgrader, P., Ryvkin, P., Bent, Z.W., Wilson, R., Ziraldo, S.B., Wheeler, T.D., McDermott, G.P., Zhu, J., et al. (2017). Massively parallel digital transcriptional profiling of single cells. Nat. Commun. *8*, 14049. https://doi.org/10.1038/ncomms14049.

68. Hao, Y., Hao, S., Andersen-Nissen, E., Mauck, W.M., 3rd, Zheng, S., Butler, A., Lee, M.J., Wilk, A.J., Darby, C., Zager, M., et al. (2021). Integrated analysis of multimodal single-cell data. Cell *184*, 3573–3587.e29. https://doi.org/10.1016/j.cell.2021.04.048.

69. Trapnell, C., Cacchiarelli, D., Grimsby, J., Pokharel, P., Li, S., Morse, M., Lennon, N.J., Livak, K.J., Mikkelsen, T.S., and Rinn, J.L. (2014). The dynamics and regulators of cell fate decisions are revealed by pseudotemporal ordering of single cells. Nat. Biotechnol. *32*, 381–386. https://doi.org/10.1038/nbt.2859.

70. Traag, V.A., Waltman, L., and Van Eck, N.J. (2019). From Louvain to Leiden: guaranteeing well-connected communities. Sci. Rep. *9*, 5233. https://doi.org/10.1038/s41598-019-41695-z.

71. Subramanian, A., Tamayo, P., Mootha, V.K., Mukherjee, S., Ebert, B.L., Gillette, M.A., Paulovich, A., Pomeroy, S.L., Golub, T.R., Lander, E.S., and Mesirov, J.P. (2005). Gene set enrichment analysis: a knowledge-based approach for interpreting genome-wide expression profiles. Proc. Natl. Acad. Sci. USA *102*, 15545–15550. https://doi.org/10.1073/pnas.0506580102.

STAR★METHODS

KEY RESOURCES TABLE

REAGENT or RESOURCE	SOURCE	IDENTIFIER
Antibodies		
Anti-mouse CD45 AF700 (clone: 30-F11)	BioLegend	Cat# 103128; RRID: AB_493715
Anti-mouse CD3ε PE (clone: 145-2C11)	eBioscience	Cat# 12-0031-83; RRID: AB_465496
Anti-mouse CD3ε BUV395 (clone: 145-2C11)	BD Biosciences	Cat# 563565; RRID: AB_2738278
Anti-mouse TCRβ FITC (clone: H57-597)	eBioscience	Cat# 11-5961-85; RRID: AB_465323
Anti-mouse TCRβ PerCP-Cy5.5 (clone: H57-597)	eBioscience	Cat# 45-5961-82; RRID: AB_925763
Anti-mouse CD8α PE-Cy7 (clone: 53–6.7)	eBioscience	Cat# 25-0081-82; RRID: AB_469584
Anti-mouse CD8α PerCP-Cy5.5 (clone: 53–6.7)	eBioscience	Cat# 45-0081-82; RRID: AB_1107004
Anti-mouse CD8α BV650 (clone: 53–6.7)	BioLegend	Cat# 100741; RRID: AB_11124344
Anti-mouse CD8β PE (clone: H35–17.2)	eBioscience	Cat# 12-0083-83; RRID: AB_657767
Anti-mouse CD4 BV605 (clone: RM4-5)	BioLegend	Cat# 100547; RRID: AB_11125962
Anti-mouse PD-1 BV421 (clone: RMP1-30)	BioLegned	Cat# 109121; RRID: AB_2687080
Anti-mouse PD-1 BV785 (clone: RMP1-30)	BioLegned	Cat# 135225; RRID: AB_2563680
Anti-mouse PD-1 APC (clone: 29F.1A12)	BioLegend	Cat# 135210; RRID: AB_2159183
Anti-mouse CD62L PerCP-Cy5.5 (clone: MEL-14)	eBioscience	Cat# 45-0621-82; RRID: AB_996667
Anti-mouse CD62L APC (clone: MEL-14)	eBioscience	Cat# 17-0621-82; RRID: AB_469410
Anti-mouse/human CD44 PE-Cy7 (clone: IM7)	eBioscience	Cat# 25-0441-82; RRID: AB_469623
Anti-mouse CD25 PE-Cy7 (clone: PC61.5)	eBioscience	Cat# 25-0251-82; RRID: AB_469608
Anti-mouse NK1.1 FITC (clone: PK136)	eBioscience	Cat# 11-5941-82; RRID: AB_465318
Anti-mouse CD11b APC (clone: M1/70)	eBioscience	Cat# 17-0112-82; RRID: AB_469343
Anti-mouse PD-L1 PE (clone: 10F.9G2)	BioLegend	Cat# 124308; RRID: AB_2073556
Anti-human HER2 PE (clone: 24D2)	BioLegend	Cat# 324405; RRID: AB_756121
Anti-mouse/human GzmB FITC (clone: GB11)	BioLegend	Cat# 515403; RRID: AB_2114575
Anti-mouse/human GzmB PE (clone: GB11)	eBioscience	Cat# 12-8899-41; RRID: AB_1659718
Anti-mouse/human GzmB AF700 (clone: QA16A02)	BioLegend	Cat# 372222; RRID: AB_2728389
Anti-mouse Prf PE (clone: S16009B)	BioLegend	Cat# 154405; RRID: AB_2721640
Anti-mouse/human Ki-67 APC (clone: SolA15)	eBioscience	Cat# 17-5698-82; RRID: AB_2688057
Anti-mouse Foxp3 PE (clone: FJK-16s)	eBioscience	Cat# 12-5773-82; RRID: AB_465936
Anti-mouse TIM3 BV421 (clone: RMT3-23)	BioLegend	Cat# 119723; RRID: AB_2616908
Anti-mouse 4-1BB PE-Cy7 (clone: 17B5)	eBioscience	Cat# 25-1371-82; RRID: AB_2573398
Anti-mouse/human TCF1 AF488 (clone: C63D9)	Cell Signaling	Cat# 6444S; RRID: AB_2797627
Anti-mouse EOMES PerCP-eF710 (clone: Dan11mag)	eBioscience	Cat# 46-4875-80; RRID: AB_10597455
Anti-mouse CTLA-4 PE (clone: UC10-4BP)	eBioscience	Cat# 12-1522-82; RRID: AB_465879
Anti-mouse CD27 APC (clone: LG.7F9)	eBioscience	Cat# 17-0271-81; RRID: AB_469370
Anti-human PD-1 (clone: EPR4877(2))	abcam	Cat# ab137132; RRID: AB_2894867
Anti-human CD8 (clone: 4B11)	Bio-Rad	Cat# MCA1817; RRID: AB_322868
Purified anti-mouse CD16/32 (clone: 93)	BioLegend	Cat# 101301; RRID:AB_312800
Biological Samples		
Tumor samples from metastatic colorectal and ovarian cancer patients	Severance Hospital, Asan Medical Center, and Seoul St. Mary's Hospital	IRB: 4-2017-1167 (Severance Hospital), IRB: 2017–1215 (Asan Medical Center), and IRB: KC18MDDF0139 (Seoul St. Mary's Hospital)

(*Continued on next page*)

Continued

REAGENT or RESOURCE	SOURCE	IDENTIFIER
Chemicals, Peptides, and Recombinant Proteins		
Hybrid Fc-fused recombinant human IL-7 (rhIL-7-hyFc) & formulation buffer	Donghoon Choi, Research Institute of NeoImmuneTech, Inc. (Rockville, MD, USA).	N/A
anti-human/mouse cross-reactive PD-L1 X anti-mouse CD3ε bispecific T cell engager	This paper	N/A
anti-human HER2 X anti-mouse CD3ε bispecific T cell engager	This paper	N/A
Collagenase D	Sigma-Aldrich	11088882001
DNase I	Roche	11284932001
β-mercaptoethanol	Gibco	21985
Antibiotic-Antimycotic	Gibco	15240
FectoPro	Polyplus	101000014
Ni-NTA agarose	Qiagen	30230
FTY720	Sigma-Aldrich	SML0700
DAPI	Thermo Scientific	62248
RBC lysing buffer	Sigma-Aldrich	R7757
Ghost Dye TM Violet 510	Tonbo Biosciences	13–0870
CellTrace™ Violet Cell Proliferation Kit, for flow cytometry	Thermo Scientific	C34571
Dewax solution	Leica Biosystems	AR9222
1X ANTIBODY DILUENT/BLOCK	Akoya Biosciences	ARD1001EA
1X OPAL ANTI-MS + RB HRP	Akoya Biosciences	ARH1001EA
BOND Epitope Retrieval Solution 1	Leica Biosystems	AR9961
BOND Epitope Retrieval Solution 2	Leica Biosystems	AR9640
Critical Commercial Assays		
Chromium Next GEM Single Cell 5' Kit v2	10X Genomics	PN-1000265
Next GEM Chip K Single Cell Kit	10X Genomics	PN-1000287
Dual Index Kit TT Set A	10X Genomics	PN-1000215
Chromium Single Cell Mouse TCR Amplification Kit	10X Genomics	PN-1000254
Deposited Data		
Raw data files for scRNA/TCR-seq	This paper	GEO: GSE237266
Experimental Models: Cell Lines		
MC38	kerafast	ENH204-FP
$MC38^{\Delta PD-L1}$ (PD-L1 deficient MC38)	Laboratory of Dr. Sang-Jun Ha	N/A
B16F10	ATCC	CRL-6475
CT26	ATCC	CRL-2638
$CT26^{hHER2}$	Laboratory of Dr. Sherie L. Morrison	N/A
4T1	ATCC	CRL-2539
FreeStyle™ 293-F Cells	Gibco	R79007
Experimental Models: Organisms/Strains		
Mouse: C57BL/6	The Jackson Laboratory (Bar Harbor, ME, USA)	Strain #: 000664; RRID: IMSR_JAX:000664
Mouse: Balb/c	Taconic Biosciences	N/A
Mouse: PD-L1 KO ($PD\text{-}L1^{-/-}$)	Laboratory of Dr. Lieping Chen	N/A

(*Continued on next page*)

Continued

REAGENT or RESOURCE	SOURCE	IDENTIFIER
Mouse: C57BL/6J-*Rag1*^{em10Lutzy}/J (RAG1 KO)	The Jackson Laboratory (Bar Harbor, ME, USA)	Strain #: 034159; RRID: IMSR_JAX:034159
Software and Algorithms		
Cell Ranger software v4.0.0	G. X. Y. Zheng et al.	N/A
Seurat v4.1.0	Y. Hao et al.	https://satijalab.org/seurat/articles/install.html
Monocle3 v.0.2.3.0	C. Trapnell et al.	https://bioconductor.org/packages/release/bioc/html/monocle.html
GSEA software v.4.1.0	A. Subramanian et al.	https://www.gsea-msigdb.org/gsea/downloads.jsp
clusterProfiler v3.16.1	G. Yu et al.	https://bioconductor.org/packages/release/bioc/html/clusterProfiler.html
Metascape	Y. Zhou et al.	https://metascape.org/
Prism software	GraphPad	https://www.graphpad.com/scientific-software/prism/
FlowJo v10	BD	https://www.flowjo.com/solutions/flowjo/downloads
Other		
Fetal Bovine Serum (FBS)	Hyclone	SV30207.02
eBioscience Foxp3/Transcription Factor Staining Buffer Set	ThermoFisher	00-5523-00
Newborn Calf Serum (NBCS)	Gibco	26010–074
DMEM	Welgene	LM001-05
RPMI-1640	Welgene	LM001-01

RESOURCE AVAILABILITY

Lead contact

Further information and requests for resources and reagents should be directed to and will be fulfilled by the lead contact, Seung-Woo Lee (sw_lee@postech.ac.kr).

Materials availability

Bispecific T cell engagers generated in this study are available from Dae Hee Kim (kimdh@kangwon.ac.kr) upon request through the Materials Transfer Agreement.

Data and code availability

- scRNA-seq data have been deposited at the GEO database and are publicly available under accession code GSE237266 as of the date of publication.
- This paper does not report the original code.
- Any additional information required to reanalyze the data reported in this paper is available from the lead contact upon request.

EXPERIMENTAL MODEL AND STUDY PARTICIPANT DETAILS

Mice

Seven to 9-week-old female C57BL/6 and Balb/c mice were purchased from ORIENT BIO Inc. or Hanabiotech (Republic of Korea). PD-L1$^{-/-}$ mice were provided by Dr. S.J. Ha (Yonsei University, Republic of Korea). PD-L1$^{-/-}$ mice were originally generated by Lieping Chen.[62] Animals were bred and maintained under specific pathogen-free conditions in the animal care facility of POSTECH Biotech Center. Housing conditions were: 12 h dark/light cycle, temperature 21°C, humidity 30–60%. All animal care and experiments were carried out in accordance with National Institutes of Health guidelines for the Care and Use of laboratory animals under protocols approved by the Institutional Animal Care and Use Committee (IACUC) guidelines of POSTECH (POSTECH-2022-0052).

Cell lines

Murine tumor cell lines, MC38 (derived from C57BL/6 colon adenocarcinoma), B16F10 (C57BL/6 skin melanoma), CT26 (Balb/c colon carcinoma), and 4T1 (Balb/c mammary adenocarcinoma) were kindly provided by Y.C. Sung (Genexine, Inc., Republic of Korea).

PD-L1-deficient MC38 ($MC38^{\Delta PD-L1}$) was kindly provided by Dr. S.J. Ha (Yonsei University, Republic of Korea). $CT26^{hHER2}$ was kindly provided by Dr. S.W. Kim (SL BIGEN, Inc., Republic of Korea). $CT26^{hHER2}$ was originally generated by S L Morrison.[63] MC38, $MC38^{\Delta PD-L1}$, and B16F10 cells were cultured in complete Dulbecco's modified Eagle's medium (DMEM) (Welgene, LM001-05) supplemented with 10% FBS (Hyclone, SH30084.03) and Antibiotic-Antimycotic (Gibco, 15240). 4T1, CT26, and $CT26^{hHER2}$ cells were cultured in complete RPMI-1640 (Welgene, LM001-01) with 2-mercaptoethanol (Gibco, 21985). All tumor cells were cultured at 37°C with 5% CO_2.

Human studies

Patients enrolled in this study have locally advanced, recurrent, or metastatic incurable tumors for whom standard therapy does not exist, has proven ineffective or intolerable, or is considered inappropriate (NCT03478995). The patients were administered either 720 μg kg^{-1} (SB10) or 1200 μg kg^{-1} (SA10, SB12, SB13) of rhIL-7-hyFc via intramuscular injection at the indicated timepoint. This study was approved by 3 institutions and complied with all relevant ethical regulations: Severance Hospital (IRB: 4-2017-1167), Asan Medical Center (IRB: 2017–1215), and Seoul St. Mary's Hospital (IRB: KC18MDDF0139). All patients provided written informed consent for the collection of tissue for research. The tumor tissues were collected during the screening phase (pre) and at the indicated time point after administration (post) for the multiplex imaging analysis. Clinical tumor biopsy samples applied a sequential approval process per institution for library preparation.

METHOD DETAILS

Study design

Here, we sought to investigate the combination of rhIL-7-hyFc and TCE as an optimal immunotherapy strategy in solid tumors by modifying the CD8 T cell landscape in tumors. Single-cell RNA-seq analyses paired with scTCR-seq of CD8 TILs were performed to characterize the differentiation and functions of CD8 subsets, including tumor-reactive and bystander cells, by the treatment of rhIL-7-hyFc and TCE. To validate the effects of the treatments on CD8 T cells, we performed flow cytometry analysis of CD8 TILs and *ex vivo* co-culture experiments with CD8 TILs and tumor cells. We used several solid tumor models to evaluate the antitumor efficacy of the combined administration of rhIL-7-hyFc and TCEs. We also analyzed CD8 TILs by IHC in clinical samples from cancer patients treated with rhIL-7-hyFc as a comparison with preclinical results. The sample size was empirically determined to be a statistically significant quantity based on the outcomes of previous research—generally, experiments aimed to include 6 to 8 mice per group. Two to three replicates were performed for each experiment, with the correct number for each experiment provided in the figure legend. Mice were randomized before starting treatments. Except when evaluating the size of the tumor, the researchers were not blinded. Outliers in the data were included.

Generation of bispecific T cell engagers

Anti-human/mouse cross-reactive PD-L1 (clone: KL001-13) variable domains were obtained by phage display as previously described.[64] Anti-human HER2 (clone: trastuzumab)[65] and anti-mouse CD3ε (clone: 145-2c11)[66] variable domains were codon optimized and synthesized commercially (Macrogen, Republic of Korea). A flexible linker ($(GGGGS)_3$) was used to fuse VL-VH (anti-human/mouse PD-L1, anti-human HER2) or VH-VL (anti-mouse CD3ε), and a flexible linker ((GGGGS)1) was used to fuse anti-human/mouse PD-L1 (VL-VH) scFv × anti-mouse CD3ε (VH-VL) or anti-human HER2 × anti-CD3ε (VH-VL) by overlap extension PCR. These bispecific fragments were constructed with Hisx6 affinity tags at their C terminus for purification. These constructs were cloned into the expression vector pCEP4 and confirmed by DNA sequencing. Purified plasmid DNA was transfected into FreeStyle 293-F Cells (Gibco, R79007) by FectoPro (Polyplus, 101000014) following the manufacturer's instructions. Cells were cultured for 5 days after transfection, and the supernatants from transfected cells were purified by open-column affinity chromatography using Ni-NTA agarose (Qiagen, 30230). Elution fractions were collected and dialyzed against PBS (pH 7.2) by Slide-A-Lyzer cassettes (Thermo Scientific, 66810). Protein concentration was determined with a NanoDrop ND-2000 spectrophotometer (Thermo Scientific) based on absorption at 280 nm. The purity of the protein was confirmed using SDS-PAGE and Coomassie brilliant blue staining.

Mouse tumor models and treatments

1×10^5 MC38 or 5×10^5 B16F10 cells resuspended in FBS-free DMEM were subcutaneously inoculated into the right flanks of C57BL/6 mice. 1×10^5 4T1 or CT26, or $CT26^{hHER2}$ cells resuspended in FBS-free RPMI-1640 were subcutaneously inoculated into the right flanks of Balb/c mice. Tumor volume was measured twice a week by the longest diameter (*a*) and perpendicular diameter (*b*) and calculated as $0.5ab$.[2] When the tumor grew to 2–4 mm in longest diameter for palpable or approximately 100 mm^3 for the advanced model, mice were randomized to the treatment with 1.25 mg kg^{-1} or 10 mg kg^{-1} rhIL-7-hyFc, kindly supplied by NeoImmuneTech, Inc. (Rockville, USA) via the Research Institute of NeoImmuneTech (Republic of Korea). rhIL-7-hyFc, a long-acting recombinant human IL-7 fused with a hybrid Fc, is a fusion protein comprising human IL-7 fused to a hybrid Fc (hyFc) region, which extends the half-life of rhIL-7-hyFc. The Chinese Hamster Ovary (CHO) cell line DG44 is used to produce rhIL-7-hyFc. Produced rhIL-7-hyFc is purified by multiple chromatography and filtration steps to achieve high purity and efficacy. Purified rhIL-7-hyFc Drug Substance (DS) is filled into glass vials, which contain active ingredient (rhIL-7-hyFc), sucrose, D-sorbitol, tri-sodium citrate dehydrates, citric acid monohydrate, and polysorbate 80 (PS80) as a stabilizer and buffer. The use of rhIL-7-hyFc in our mouse models is based on

evidence from previous researches demonstrating its efficacy and functional compatibility in murine systems.[34,36] TCEs were treated intravenously or intratumorally 3 days after rhIL-7-hyFc treatment. To block T cell migration, FTY720 (Sigma, SML0700) (60 μg/head) was administered intraperitoneally (i.p.) for a total of 10 times on days 5, 6, 8, 10, 12, 14, 16, 18, 20, and 22. Mice were euthanized when tumor size reached a diameter of 20.0 mm length.

Multiplex immunofluorescence staining and analysis

Immunofluorescence stain, scan, and analysis were performed on prismCDX Co., Ltd (Republic of Korea). Four μm sections of specimens were cut from FFPE blocks. Slides were heated for at least 1 h in a dry oven at 60°C, followed by multiplex immunofluorescence staining with a Leica Bond Rx Automated Stainer (Leica Biosystems, Germany). Briefly, the slides were deparaffinized with Leica Bond Dewax solution (Leica Biosystems, AR9222), followed by antigen retrieval with Bond Epitope Retrieval (Leica Biosystems, AR9640). The staining proceeds in sequential rounds of blocking with antibody diluent solution (Akoya Biosciences, ARD1001EA), followed by primary antibody and OPAL polymer HRP (Akoya Biosciences, ARH1001EA) incubation for 30 and 10 min, respectively. Visualization of antigen was accomplished using tyramide signal amplification for 10 min, after which the slide-treated Bond Epitope Retrieval (Leica Biosystems, AR9961) to remove bound antibodies before the next step. The process from the blocking to the antigen retrieval is repeated for each antibody staining. Nuclei were stained with DAPI (Thermo Scientific, 62248) for counterstaining. All the slides were covered by Prolong Gold antifade reagent (Invitrogen, P36935). The primary antibodies used were as follows: anti-PD-1 (Abcam, ab137132) and anti-CD8 (Bio-rad, MCA1817). Multiplex stained slides were scanned using the Vectra Polaris Automated Quantitative Pathology Imaging System (Akoya Biosciences) at 20× magnification. Then, an algorithm was created in the Inform Image Analysis software. Based on DAPI staining, every single cell was segmented, and phenotyping was performed according to each marker's expression compartment and intensity. After designating the region (ROI, region of interest) to be analyzed on the whole tissue image, the same algorithm created in this way was applied and batch-running. The exported data is consolidated and analyzed in R software.

Single cell preparation

Tumor tissues were mechanically dissected and then digested with 400 units/mL collagenase D (Roche, 11088882001) and 200 μg/mL DNase I (Roche, 11284932001) in washing buffer (2% newborn calf serum (Gibco, 26010–074) plus antibiotic-antimycotic in RPMI-1640) for 30 min in a shaking incubator at 37°C. The enzyme-digested tumor tissues were dissociated into a single-cell suspension using a 70 μm cell strainer. Spleens and tumor-draining lymph nodes (tdLN) were mechanically dissociated by passage through a 70 μm cell strainer. Red blood cells (RBCs) in spleens were lysed with RBC lysing buffer (Sigma-Aldrich, R7757). Peripheral blood (PB) was collected and analyzed for a complete blood count (CBC) with a VetScan HM2 analyzer (Abaxis, Inc.). Cell counts of single-cell suspension were determined using a Vi-CELLTM XR analyzer (Beckman Coulter, Inc.).

Single-cell RNA sequencing

CD8 T cells from the single cell suspensions of tumors were enriched positively with IMag according to the manufacturer's protocol or sorted using flow cytometry (MoFlo Astrios EQ Cell Sorter, Beckman Coulter Life Science) based on surface marker expression ($GhostDye^{-}CD45^{+}TCR\beta^{+}CD8\beta^{+}$). scRNA-seq analyses were performed by Macrogen, Inc. (Republic of Korea).

Preprocessing of scRNA-seq data

10× Genomics Cell Ranger (v.4.0.0 for Buffer vs. rhIL-7-hyFc comparison and v.6.1.2 for rhIL-7-hyFc vs. combination (rhIL-7-hyFc + TCE))[67] was used to align reads and count the single-cell sequencing data using the GRCm38 as the reference genome: 'cell ranger count' and 'cell ranger vdj' pipelines were applied to process scRNA-seq and scTCR-seq, respectively, that led to generating features, barcodes, and matrices. Cells expressing fewer than 200 genes were excluded, and genes detected in more than two cells were counted. Additionally, cells with more than 5% mitochondrial gene counts [calculated as UMIs (unique molecular identifier) from mitochondrial genes divided by total UMIs] and doublet cells expressing more than 6,000 genes were excluded. CD8 T cells were identified as those expressing *Ptprc* and *Cd3*, while not *Cd68*, *H2-Aa*, and *H2-Eb1*. As a result, 6,639 cells for Buffer vs. rhIL-7-hyFc and 10,920 cells for rhIL-7-hyFc vs. combination (rhIL-7-hyFc + TCE) were left for further downstream analysis.

Annotation of cell types and identification of differentially expressed genes

Seurat software (v.4.1.0)[68] was used to analyze three outputs generated by the Cell Ranger pipeline: barcodes, features, and matrices. The following steps were performed: (i) normalizing and log-transforming the counts with the NormalizeData function, (ii) selecting 2000 highly variable genes with the FindVariableFeatures function, (iii) integrating the data with the FindIntegrationAnchor function by finding anchor genes through a canonical correlation analysis (CCA) algorithm using the 2000 genes, then performing principal component analysis (PCA) with RunPCA function, (iv) reducing dimensionality with RunUMAP function to create UMAP plot, (v) clustering cells with the FindClusters function by setting resolution size to 0.3, (vi) annotating cell types with selected markers such as *Pdcd1* (tumor-reactive), *Tcf7* (bystander), etc., as described in Figure 1B, while mapping TCRseq information to the reference genome to identify different types of T cells.

DEGs were estimated using FindMarkers from the comparison of gene expression between two different sets of comparisons, i.e., (i) between Buffer and rhIL-7-hyFc, and (ii) between rhIL-7-hyFc and Combo. The criteria for DEGs were a $\log_2$ fold change greater than 0.25 and an adjusted *p* value less than 0.05 (by two-tailed Student's t test).

Trajectory and pseudo-time analysis

The trajectory/pseudo-time analysis was performed using the R package Monocle 3 (v.0.2.3.0).[69] The method used for dimensionality reduction was 'UMAP', where cells were clustered using the Leiden algorithm,[70] with the clustering resolution parameter set at 0.001. Cluster 1, which expressed the highest levels of naive/central memory marker genes, was set as the root cell for the order_cells function.

GO analysis and GSEA

GO analysis was performed on DEGs identified by comparing gene expression between rhIL-7-hyFc-treated and combo-treated cells in each of the bystander, transitional, and tumor-reactive groups. The Metascape web tool (https://metascape.org/) was utilized for GO analysis. GSEA was conducted using GSEA software (v.4.1.0)[71] on the normalized matrix of cells, employing the 'No_Collapse' option and 'Permutation type = phenotype' option. Visualization of the GSEA results was performed using the Enrichplot package (v.1.8.1). (https://github.com/GuangchuangYu/enrichplot).

T cell activation assay

For PD-L1×CD3 TCE functional assay, splenocytes (effector cells) from naive PD-L1-deficient mice (PD-L1$^{-/-}$) were co-cultured with CTV-labeled target cells (MC38 or MC38$^{\Delta PD-L1}$) in the presence of PD-L1×CD3 TCE (E:T = 20:1). For HER2×CD3 TCE functional assay, CTV-labeled CT26 or CT26^{hHER2} target cells and splenocytes (effector cells) from naive Balb/c mice were co-cultured in the presence of HER2×CD3 TCE (E:T = 20:1). After 48 h, T cell activation and cytotoxicity was analyzed by flow cytometry. The CTV^{+} Ghost Dye^{-} cells were regarded as viable target cells. Cytotoxicity was determined as follows: % cytotoxicity = (percentage of viable target cells when TCE is absent – the percentage of viable target cells when TCE is present)/(percentage of viable target cells when TCE is absent) × 100.

For the *ex vivo* T cell activation assay, MC38 tumor-bearing C57BL/6 mice were treated s.c. with rhIL-7-hyFc (10 mg kg^{-1}). After 7 days of treatment, FACS-sorted PD-1^{-} and PD-1^{+} CD8 T cells from the single cell suspensions of tumors were co-cultured with CTV-labeled MC38 target cells in the presence of TCE (E:T = 10:1). After 48 h, T cells activation and cytotoxicity were analyzed by flow cytometry.

Flow cytometry

Single-cell suspensions were first stained with Ghost Dye TM Violet 510 (Tonbo Biosciences, 13–0870) according to the manufacturer's protocol to exclude dead cells. Cells were stained with anti-mouse CD16/32 (clone 93) to block non-specific Fc receptor binding and then stained with the fluorescence-conjugated antibodies against surface molecules at 4°C for 20 min. Flow cytometry antibodies used in this study are listed in the Key resources table. Cells were fixed and permeabilized for intracellular staining (ICS) using the Foxp3/Transcription factor staining buffer set (eBioscience) according to the manufacturer's protocol and then stained with antibodies against intracellular molecules. Data were acquired with CytoFLEX (Beckman Coulter) in the Microbiome Core Research Support Center of Korea Basic Science Institute (KBSI) (2021R1A6C101A390) and analyzed using FlowJo software (TreeStar Inc.).

QUANTIFICATION AND STATISTICAL ANALYSIS

The statistical analysis was assessed using Prism 9 software (GraphPad Software). Data were presented as means ± SEM. As indicated in the figure legends, *p*-values were described as shown: $^{*}p < 0.05$, $^{**}p < 0.01$, $^{***}p < 0.001$, and $^{****}p < 0.0001$. ns, not significant.